
GAZİ ÜNİVERSİTESİ
Gazi
1926

THE NUMERICAL MAGNETO-THERMAL ANALYSIS ON TRANSFORMER COVERS PLATE

A THESIS SUBMITTED TO
THE GRADUATE SCHOOL OF NATURAL AND APPLIED SCIENCES
OF
GAZİ UNIVERSITY

BY

Mohammad Zia ZAHEDI

IN PARTIAL FULFILLMENT OF THE REQUIREMENTS
FOR
THE DEGREE OF DOCTOR OF PHILOSOPHY
IN
ELECTRICAL & ELECTRONICS ENGINEERING

JANUARY 2019

The thesis study titled "THE NUMERICAL MAGNETO-THERMAL ANALYSIS ON TRANSFORMER COVERS PLATE" is submitted by Mohammad Zia ZAHEDI in partial fulfillment of the requirements for the degree of Doctor of Philosophy in the Department of Electrical-Electronics Engineering, Gazi University by the following committee.

Supervisor: Prof. Dr. İres İSKENDER

Electrical-Electronics Engineering, Çankaya University

I certify that this thesis is a graduate thesis in terms of quality and content …..……..……..

Chairman: Prof. Dr. Hamit ERDEM

Electrical-Electronics Engineering, Başkent University

I certify that this thesis is a graduate thesis in terms of quality and content …..……..……..

Member: Prof. Dr. M. Cengiz TAPLAMACIOĞLU

Electrical-Electronics Engineering, Gazi University

I certify that this thesis is a graduate thesis in terms of quality and content …..……..……..

Member: Prof. Dr. Erkan AFACAN

Electrical-Electronics Engineering, Gazi University

I certify that this thesis is a graduate thesis in terms of quality and content …..……..……..

Member: Assoc. Prof. Dr. Ahmet KARAARSLAN

Energy Systems Engineering, Ankara Yıldırım Beyazıt University

I certify that this thesis is a graduate thesis in terms of quality and content …..……..……..

Date: 10/01/2019

I certify that this thesis, accepted by the committee, meets the requirements for being a Doctor of Philosophy Thesis.

……..…….

Prof. Dr. Sena YAŞYERLİ

Dean of Graduate School of Natural and Applied Sciences

ETHICAL STATEMENT

I hereby declare that in this thesis study I prepared in accordance with thesis writing rules of Gazi University Graduate School of Natural and Applied Sciences;

- All data, information and documents presented in this thesis have been obtained within the scope of academic rules and ethical conduct,
- All information, documents, assessments and results have been presented in accordance with scientific ethical conduct and moral rules,
- All material used in this thesis that are not original to this work have been fully cited and referenced,
- No change has been made in the data used,
- The work presented in this thesis is original,

or else, I admit all loss of rights to be incurred against me.

Mohammad Zia ZAHEDI
10/01/2019

THE NUMERICAL MAGNETO-THERMAL ANALYSIS ON TRANSFORMER COVERS PLATE

(Ph. D. Thesis)

Mohammad Zia ZAHEDI

GAZİ UNIVERSITY

GRADUATE SCHOOL OF NATURAL AND APPLIED SCIENCES

January 2019

ABSTRACT

High currents conductors at the low voltage side of transformers cover are sources of losses and thermal problems in the tank cover. Considering the advantages of Finite Difference Method (FDM) as; being more flexible to deal with the nonlinear constitutive law, being most popular method for simple geometry regions and low-cost computational procedure and being easy-to-be implemented, the FDM is used to find an exact estimation of losses at the cover bushing region considering its non-linear behavior. In FDM approach, transient solution of Maxwell's equations and Ohm law is done at the cross section area in the axial symmetry page of a steel disk and then, two-level Adaptive Mesh Refinement (AMR) technique is applied to magnetic FD analysis of the problem in the steady state condition. The thermal analysis of the cover plate is performed using the Alternating Direction Implicit (ADI)-FD method. The combination of AMR and ADI-FDM proposes a solution algorithm, which improves the accuracy and decreases the computational time of the analyses. The reliability of the proposed techniques has been confirmed by results of experimental works and finite element method (FEM). This study also proposes a linear and non-linear 3D FEM optimization design of cover plates for a 1600kVA, 400V 3-phase distribution transformer, using a suitable geometry of Stainless Steel Insert (SSI) to overcome the local overheating and to keep the temperature below 140°C. The applied linear approximations for calculation of losses and temperature is sufficiently fast such that the computations can be performed in a moderate computer resource. In addition, a set of analytical formula extracted from 3D FEM simulations results has been proposed for estimating the hot spot temperature in the cover plate of distribution transformer in this study. Numerous FEM simulations are carried out to compute the temperature in the carbon steel of the tank cover for different cases of with and without SSI. In summary, the numerical magneto-thermal analysis on the transformer cover plate has been done using FEM-FEM, FDM-FEM and Adaptive-FDM-ADI-FDM coupling approach in the frame of MATLAB and ANSYS software.

Science Code : 90514

Key Words : Eddy current losses, hot spot temperature, finite difference method, alternating direction implicit, adaptive mesh refinement, finite element simulation, transformer cover, stainless steel insert and bushing regions

Page Number : 100

Supervisor : Prof. Dr. İres İSKENDER

TRANSFORMATÖR KAPAĞINDA NÜMERİK MANYETO-TERMAL ANALİZİ

(Doktora Tezi)

Mohammad Zia ZAHEDI

GAZİ ÜNİVERSİTESİ

FEN BİLİMLERİ ENSTİTÜSÜ

Ocak 2019

ÖZET

Transformatör kapağının alçak gerilim bölgelerindeki yüksek akım iletkenleri, kazan kapağındaki kayıpların ve termal problemlerin kaynaklarıdır. Sonlu farklar yönteminin (FDM) lineer olmayan bünye denklemi ile başa çıkmada daha esnek olduğunu, kolay uygulanabileceğini, basit geometrili bölgeler için en popüler yöntem olduğunu ve düşük maliyetli hesaplama metodu olduğu gerçekleri göz önüne alındığında, FDM yaklaşımı buşing bölgesindeki kayıpları kapağın lineer olmayan davranışını da hesaplayarak en yakın tahminini bulmada kullanılır. FDM yaklaşımında, Maxwell denklemlerinin ve Ohm yasasının geçici çözümü, bir çelik diskin eksenel simetrik bölgesindeki kesit alanında yapılır. Bir sonraki adımda, kararlı haldeki problemde manyetik FD analizine 2 seviyeli AMR teknolojisi uygulanmaktadır. Kapağın termal analizini ADI-FD metod yardımıyla yapılır. AMR ve ADI-FDM kombinasyonu ile önerilen çözüm algoritması, analizlerinin doğruluğu arttırıp hesaplama süresini azaltılmaktadır. Önerilen yöntemlerin güvenilirliği deneysel sonuçlar ve sonlu elemanlar yöntemi (FEM) analizi ile doğrulanmıştır. Bu çalışma aynı zamanda, bölgesel aşırı ısınmanın üstesinden gelmek ve kapak sıcaklığını 140°C'nin altında tutmak için uygun bir paslanmaz çelik malzeme (SSI) geometrisi kullanarak, 3-fazlı dağıtım trafoları için kapak levhalarının lineer/lineer olmayan 3D FEM optimizasyon tasarımı önermiştir. Kayıplar ve sıcaklık hesaplamaları için uygulanan lineer yaklaşımlar yeterince hızlıdır, ki bu hesaplamalar orta seviye bir bilgisayarla gerçekleştirilebilir. Ayrıca, bu çalışmada, dağıtım trafolarının kapak levhasındaki kızgın nokta sıcaklığını tahmin etmek için 3D FEM simülasyonlarından elde edilen souçları kullanarak bir dizi analitik formül önerilmiştir. SSI ve SSI olmadan durumlarda, karbon çeliğinden kazan kapağının sıcaklığını hesaplamak için çok sayıda FEM simülasyonu gerçekleştirilmiştir. Kısaca, trafo kapak levhasında nümerik manyeto-termal analizi, MATLAB ve ANSYS yazılımları kullanılarak, FEM-FEM, FDM-FEM ve Adaptif-FDM-ADI-FDM birleştirme yaklaşımı ile yapılmıştır.

Bilim Kodu	:	90514
Anahtar Kelimeler	:	Edi akımı kayıpları, sıcak nokta sıcaklığı, sonlu fark yöntemi, değişen yönlü kağalı (ADİ), adaptif mesh arıtma, sonlu eleman simulasyonu, transformatör kapağı, paslanmaz çelik atma ve buşing bölgeleri
Sayfa Adedi	:	100
Danışman	:	Prof. Dr. İres İSKENDER

ACKNOWLEDGEMENTS

All praise be to Allah, Lord of all the worlds.

CONTENTS

Page

Page

LIST OF TABLES

Table **Page**

Table **Page**

LIST OF FIGURES

Figure **Page**

Figure **Page**

Figure **Page**

Figure **Page**

Figure **Page**

SYMBOLS AND ABBREVIATIONS

The symbols and abbreviations used in this study are presented below along with explanations.

Symbols	Explanations
a	Hole radius
$\mathbf{B}$	Magnetic flux density
B_r	Radial flux density
B_z	Axial flux density
B_φ	Azimuthal component of the magnetic flux density
b	Disk radius
C_p	Specific heat
c	Disk Thickness
f	Frequency
$\mathbf{H}$	Magnetic field intensity
Hz	Hertz
$H\varphi$	Azimuthal component of the magnetic field intensity
h_1	Distance between a typical point and the right neighbor point
h_2	Distance between a typical point and the left neighbor point
h_3	Distance between a typical point and the up neighbor point
h_4	Distance between a typical point and the bottom neighbor point
h_c	Convection heat transfer coefficient
I	RMS current
I_m	Peak value of current
$\mathbf{J}$	Current density
k	Thermal conductivity
N_r	Mesh number at r-direction
N_z	Mesh number at z-direction
n	n^{th} time step

Symbols	Explanations
T	Temperature of the cover steel
T_a	Ambient temperature
δ	Skin depth
ε_r	Emissivity coefficient of the radiation heat transfer
μ	Magnetic permeability
ρ	Mass density
σ	Electrical conductivity
σ_r	Stefan–Boltzmann constant

Abbreviations	Explanations
2D	Two dimension
3D	Three dimension
ADI	Alternating Direction Implicit
AM	Analytical method
AMR	Adaptive Mesh Refinement
BC	Boundary Condition
FD	Finite Difference
FDM	Finite Difference Method
FE	Finite Elements
FEM	Finite Elements Method
PDE	Partial Differential Equation
RMS	Root mean square
SSI	Stainless Steel Insert

1. INTRODUCTION

Transformers are one of inevitable components of a power system, in the spite of this fact that transformers have small losses or high efficiency, there are significant number of them in any power system. So that, they have an unbelievable role in the environment pollution due to consuming energy as losses cause more emissions of carbon dioxide. Taking into account the large number of transformers, small reduction in the losses have a vital role. In addition, the study of tank cover losses of transformers due to high current bushings is also important for preventing local overheating in the cover [1].

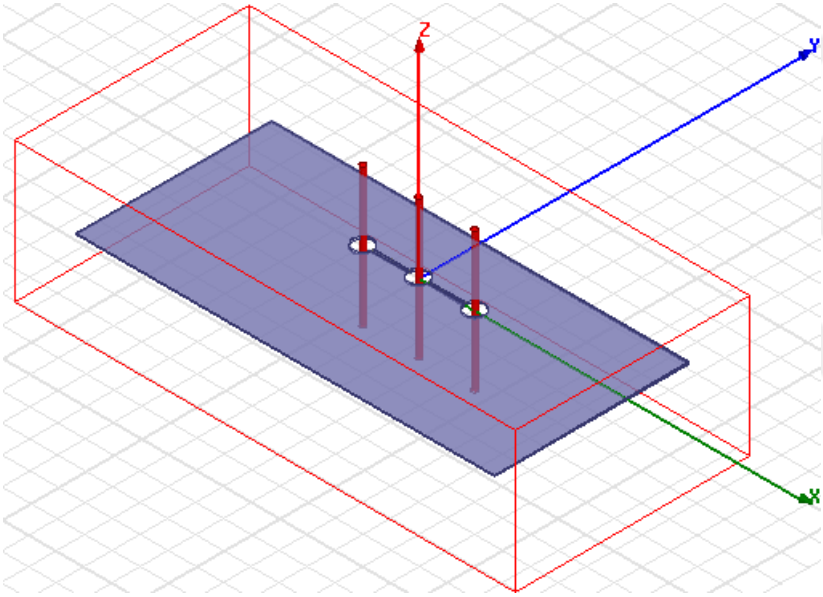

Figure 1.1. The tank cover plate, low voltage side conductors and SSI slit of a 3-phase transformer

High spot temperatures arise in the tank cover of distribution transformers because of high current leads (Figure 1.1). The induced eddy currents cause overheating of the cover steel nearby bushings, which can degrade transformer oil and damage the painting of the cover [2-5]. These damages can be caused to a significant fault in transformers [6, 7]. In the design of tank cover, the minimization of heating hazard on transformer plays an important role to improve useful life and cost savings of electrical services. The most important criterion of a transformer cover plate design is to decrease hot spot temperature and to keep it below 140°C to avoid degradation oil and gases production [8-11]. This criteria could be achieved by reducing the cover plate losses. One of the most effective ways is to use a suitable geometry

of stainless steel insert (SSI) between the bushings, which has a high electrical resistance [10, 12-14].

Besides, the application of advanced methods to find out an exact estimation of magnetic field, eddy losses and the temperature distributions in tank cover steel plates is of great interest [15].

The magnetic field analysis of the cover of power transformers has been done based on Poynting's theorem or Maxwell's equations in different methods, such as numerical, analytical and semi-analytical methods (AMs) for the case of linear/non-linear magnetic permeability of the steel. Turowski according to Poynting's theorem has proposed a semi-analytical equation for the losses calculation in any cases, linear or nonlinear magnetic permeability, using two semi-empirical parameters [10]. At the Maxwell's equations based solutions, linear FEM [5, 12, 13], AM [16, 17] are used for analyzing the transformer cover. The AM based solution of losses[16] has showed that the applied approach has acceptable results, despite of neglecting so small axial eddy currents. Besides, some authors used surface impedance boundary condition as a result of Poynting's theorem for the fast calculation of transformer tank losses, taking into account the linear permeability of the tank steel, which has a good agreement with experimental results[14, 16, 18]. Recently, the non-linear property of permeability has been taken into account in different methods, such as FEM [19], FDM [20] and AM [21], to obtain a precise estimation of the eddy losses of cover plate. Actually, it is impossible to find an analytical solution of magnetic field for a problem with a complex geometry, especially at non-linear cases.

The direct measurement of the eddy losses of a transformer cover is not possible, therefore; it is rather difficult to verify the given losses results from magnetic analysis. So that, the consequences of the magnetic analysis are used not only in estimation of the losses but also in approximation of the temperature distribution. Thermal analysis of cover plate has also been done by using FEM [5, 19, 22, 23] and AM [15], where, losses have been imported, as heat source, from the magnetic analysis into the thermal steady state analysis. The magneto-thermal analyses have been implemented in the form of linear FEM-FEM [5], linear semi analytical-FEM [22, 23] and nonlinear semi analytical-FEM [22, 23] coupling. Some authors

have been used calibration processes, which provide the precise value of magneto-thermal data, to ensure the accuracy of given results [22, 23].

Non-linear FD analysis of transformer tank has been done in [20] by using one dimension (1D) FDM limited to a special stability situation.

In this study, 2D FD analysis on transformers cover is preferred because of three reasons: it is more flexible to deal with the nonlinear constitutive law, it is most popular method for simple geometric regions, it is easy to implement than the other methods. Therefore, this study proposes 2D FDM Maxwell's equations based solutions of the magnetic field and losses in transformers cover near the lead conductor, considering the linear/nonlinear behavior of the magnetic permeability of the steel and symmetry conditions of the solution area. It is not necessary to purchase special expensive software licenses and powerful computers. This study also proposes a non-linear 2D FEM thermal analysis at the same solution area of the 2D FDM magnetic analysis. In addition, a calibration procedure based on the measurement results applies between the two analyses to ensure the precision of the results obtained from the implemented data (natural convection coefficient, thermal conductivity and electrical conductivity) in the both analyses. The reliability of the proposed technique is confirmed by experimental and FE analysis results, from the tank cover temperature point of view.

In the next step, the study proposes an adaptive magneto-thermal FD analysis near the lead conductors of transformers cover. Where, a steel disk and a conductor is used as an approximate model of the problem. The solution area is only the upper half of the cross section area in axial symmetry page of the disk. In the case of magnetic analysis, using an adaptive mesh refinement (AMR) in 2D FDM steady state solution of Maxwell equations and ohm law, considering the nonlinear behavior of the tank steel. In the thermal analysis, using alternating direction implicit (ADI)-FDM solution of the heat conduction equation in the same solution area. Besides, a calibration procedure again between magnetic and thermal analyses is used to ensure the accuracy of the achieved results by identifying the magnitude of implemented parameters in the both of the analysis according to the measurement results. Therefore, a solution algorithm is obtained by combination of AMR and ADI-FDM, which improves the accuracy and decreases the computational time of the magnetic and thermal

analysis of the cover plate. The validity of the proposed approach is certified from the cover temperature point of view by FE analysis and experimental results.

As mentioned before, the study of maximum temperature rise in the tank cover plates of transformers, because of high current bushings is the most important section in the design stage. Hence, we employ FEM simulations to assess the temperature in the cover plate of distribution transformers in a commercial FEM software such as ANSYS. Electromagnetic analysis of the tank cover is done while taking into consideration linear/nonlinear magnetic behavior of the steel plate. Subsequently, the magnetic field and eddy losses of the cover plate in the linear/non-linear behavior of the magnetic permeability of the cover steel are studied and compared to each others. The losses calculated in 3D FEM are compared with those AM and experimental results. Then thermal steady state analysis is used to figure out the temperature distribution of the tank cover under convective and radiative heat flux boundary conditions. If necessary, the hot spot temperature of the transformer cover is reduced to permissible maximum temperature by using SSI slit with suitable dimensions. The stray magnetic field losses and hot spot temperature are estimated in the case of with and without SSI. Hence an optimum tank cover design for distribution transformers can be obtained.

There are numerous numerical approximations [5, 12-14, 24, 25] have been calculated eddy losses and their thermal effects, caused by high current bushings, in tank covers. However, these methods needs more computational cost to obtain eddy losses in the thin skin depth of the cover steel. So that, a rapid solution method is needed[18] for designer to determine optimum design parameters which keep the hot spot temperature in the permission temperature.

Consequently, this study has proposed quadratic temperature functions, which can be easily used to compute the hot spot temperature of distribution transformers cover with/without SSI with good accuracy. The temperature in the tank cover is obtained using FEM simulations. The proper validation of the losses is done by using laboratory data. Therefore, a fast calculation of hot spot temperatures in tank cover of distribution transformers is proposed.

With considering the above points, this empirical research under the title of “The numerical magneto-thermal analysis on transformer covers plate” have carried out in general two parts of the methodologies (in sections 2-4) and their applications (in section 5).
The first section of the methodologies (section 2) is a brief background of the electromagnetic and thermal studies on the tank cover, in which necessary analytical equations and boundary conditions are explained in details.

The important points which has to be considered in FE analysis at the case of Eddy Current and Transient solutions is explained in section 3.

A Magneto-thermal FDM solution approach on the bushing regions of the tank cover at transient and steady state conditions have presented in section 4 by details.

In the last section, the results of the analytical and numerical application of magneto-thermal analysis on the tank cover are discussed and then compared with experimental data. An optimum design of the tank cover in linear and non-linear conditions is offered. Besides of that a set of analytic formulas for fast determination of the hot spot temperature in the tank cover is presented. Discussion about the advantages and disadvantages of the proposed method and some recommendations for future study has been given.

2. ELECTROMAGNETIC AND THERMAL BACKGROUND

2.1. Eddy Losses and Magnetic Analysis

2.1.1. Bushing region of the cover

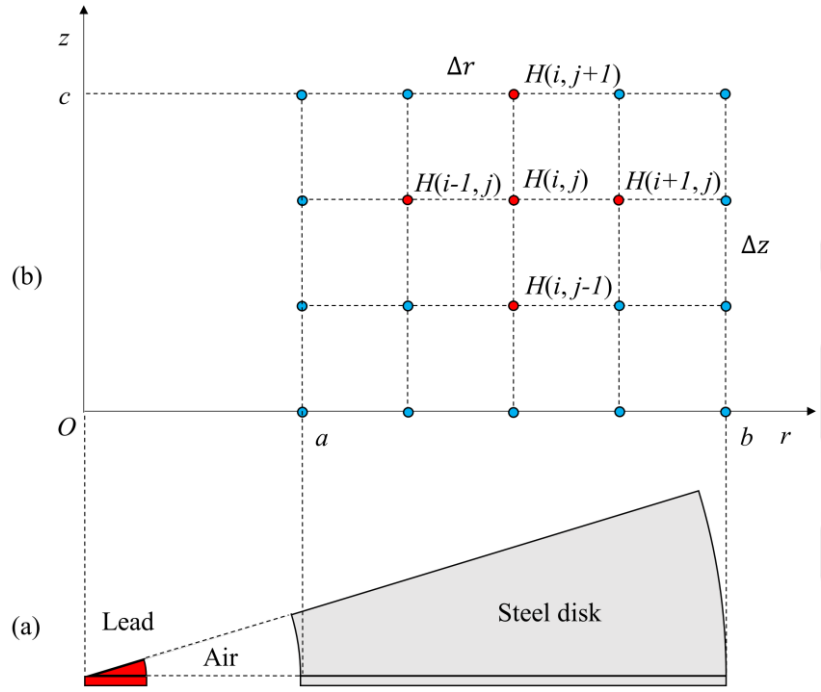

Figure 2.1. (a)The geometry, parameters, elements of the problem. (b) The computational stencil of the uniform FD mesh in magnetic analysis.

The high current conductors, passing through the bushings of the tank cover at low voltage side, create a magnetic field, which generates eddy currents with accompanying losses in the tank cover near the current carrying conductor.

Since the losses are concentrated near the bushings, the actual dimensional geometry and size of the tank cover will not matter much. Therefore, we can obtain a reasonable estimation of the cover plate losses of transformer by considering a disk steel, as shown in Figure 2.1 [16].

Combining of Ohm's law with Maxwell's equations gives a non-linear mathematical model of the magnetic field in the cover plate in a parabolic partial differential equation(PDE) form as in [20, 26], for low frequency limit.

According to Ohm's law:

$$\mathbf{J} = \sigma \mathbf{E} \tag{2.1}$$

where **J**, σ and **E** are the current density, the electrical conductivity of material and electric field intensity, respectively. According to Ampere's law:

$$\nabla \times \mathbf{H} = \mathbf{J} \tag{2.2}$$

where $\mathbf{H}$ is the magnetic field strength. Taking the curl of both sides of (2.2), then substituting Ohm's law and then using vector calculus identity of $\nabla \times \nabla \times \mathbf{H}$

$-\nabla^2 \mathbf{H} = \nabla \times (\sigma \mathbf{E})$

where $\nabla \cdot \mathbf{H} = 0$. Finally, substituting Faraday's law, $\nabla \times \mathbf{E} = -\partial \mathbf{B}/\partial t$,

$$\nabla^2 \mathbf{H} = \sigma \partial \mathbf{B}/\partial t \tag{2.3}$$

where σ is the electric conductivity of steel plate and **B**, the magnetic flux density, is related to the magnetic field intensity **H** by

$$\mathbf{B} = \mu \mathbf{H} \tag{2.4}$$

where μ is the magnetic permeability of steel plate.

It is convenient to solve (2.3) in cylindrical coordinate system, since the problem, Figure 2.1, is axisymmetric and the solution domain reduces to a rectangular area. Therefore, equation (2.3) reduces to (2.5), because the azimuthal component of Laplacian of **H** in cylindrical coordinate system is $\nabla^2 H_\varphi - H_\varphi / r^2$,

$$\frac{1}{r}\frac{\partial H_\varphi}{\partial r} + \frac{\partial^2 H_\varphi}{\partial r^2} - \frac{H_\varphi}{r^2} + \frac{\partial^2 H_\varphi}{\partial z^2} = \sigma \frac{\partial B_\varphi}{\partial t} \tag{2.5}$$

where H_φ is an azimuthal component of the magnetic field, because **H** has only azimuthal component in the given condition [16], [26].

The non-linear mathematical model of the magnetic field in the cover plate (2.5) reduces to (2.6), an elliptic PDE, taking into account the harmonical changes of the magnetic field intensity $H_\varphi(r,z,t)=H_\varphi(r,z)e^{j\omega t}$ in time with angular frequency $\omega=2\pi f$, as [16, 26].

$$\frac{1}{r}\frac{\partial H_\varphi}{\partial r}+\frac{\partial^2 H_\varphi}{\partial r^2}-\frac{H_\varphi}{r^2}+\frac{\partial^2 H_\varphi}{\partial z^2}=j\omega\sigma\mu H_\varphi \tag{2.6}$$

The Dirichlet boundary conditions(BCs) as shown in the Figure 2.2 at $r=a$, $r=b$ and $z=c/2$ surfaces are given by (2.21) which specify magnetic field intensity of cover plate uniquely, where *a*, *b* and *c* are internal, external radius and the thickness of circular tank, respectively.

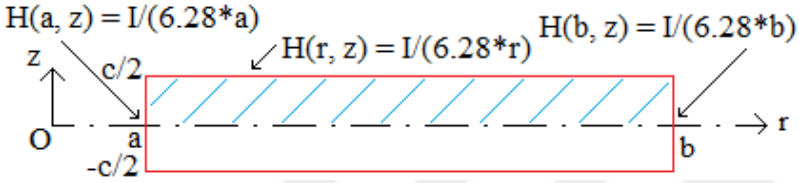

Figure 2.2. The magnetic field Dirichlet BCs of the cover plate

The non-linear numerical transient solution of the magnetic field (2.3) can be done by applying *B*-*H* curve of the cover steel at each time interval of algorithm. The cover plate material is low carbon structural steel 1010. The *B*-*H* curve of steel has been shown in Figure 2.3. The curve data have been taken from ANSYS's [27] material library. A linear interpolation fitting or a curve fitting method has been adopted to derive the relationship between *B* and *H*.

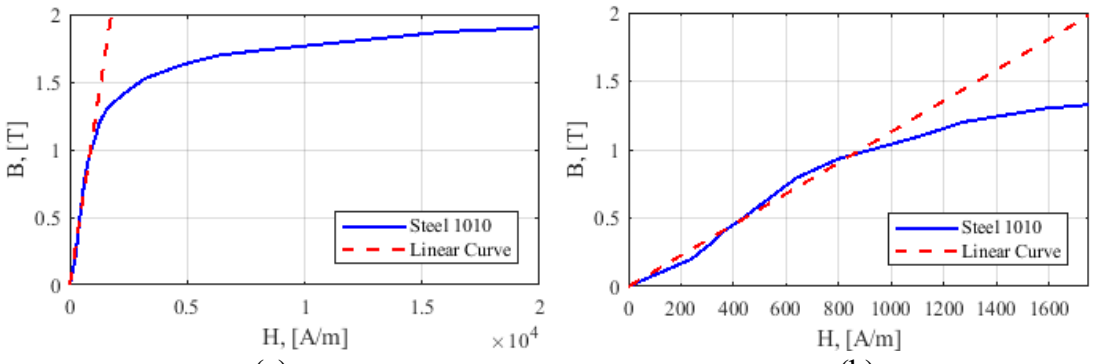

Figure 2.3. (a) *B*-*H* curve for steel 1010 compared with a linear curve (μ_r=900) and (b) Zoom-in into small magnetic fields to show detail changes.

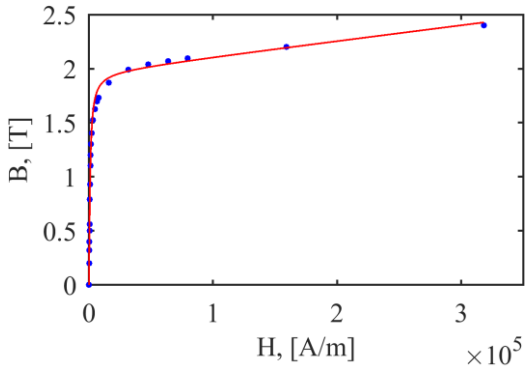

Figure 2.4. Actual and fitted *B-H* curve of steel 1010.

$$B = \mu_0 \left(a_1 \arctan\left(a_2 H \right) + a_3 H \right), \tag{2.7}$$

In the fitted curve (2.7), a_1 = 998 412.78 A/m, a_2 = 0.001 002 $(\text{A/m})^{-1}$, a_3 = 1.152 2 are parameters that have been specified by fitting equation (2.7) to actual data. At the fitting procedure, a trust region strategy developed to minimize least squares with the relative error of 1.19%. Trust region is a global strategy algorithm that improves a locally convergent algorithm, such as Newton, to a globally convergent, by using the quadratic model of objective function. Trust region, first chooses the maximum distance – the trust region radius – and then seeks both the direction and the step length that makes the best possible improvement of the function inside the trust region around the current point. [21, 28, 29].

The eddy current density (2.2) in the solution domain of the problem is determined by;

$$\mathbf{J} = -\partial H_\varphi / \partial z \, \hat{r} + \left(H_\varphi / r + \partial H_\varphi / \partial r \right) \hat{k} \tag{2.8}$$

Eddy losses density $p_v(\mathbf{r})$ at any position $\mathbf{r}$ can be find out according to (2.9) and (2.10) in transient and steady state analysis, respectively.

$$p_v(\mathbf{r}) = (1/T) \int_0^T \left(J^2(\mathbf{r}, t) / \sigma \right) dt \tag{2.9}$$

$$p_v(\mathbf{r}) = J^2(\mathbf{r}) / \sigma \tag{2.10}$$

where T is the period of electromagnetic-field oscillation and J is the eddy current density. In addition, the total eddy loss is determined by (2.11).

$$Loss = 2\pi \int_0^c \int_a^b p_v(\mathbf{r}) r dr dz \tag{2.11}$$

Linear analytical steady state solution of magnetic field can be found as

$$H_\varphi(r,z) = \frac{I}{2\pi r}\left[\frac{\cosh\left[(1+j)qz\right]}{\cosh\left[(1+j)qc/2\right]}\right] \tag{2.12}$$

where I is a root mean square (RMS) current lead and q equals $1/\delta$ which δ, the skin depth of tank steel, is given by (2.13). This result does not exactly satisfy the boundary condition (2.21) at $r=a$ surface except in the limit of small $qc/2$.

$$\delta = \sqrt{2/\omega\mu\sigma} \tag{2.13}$$

Therefore, the radial component of eddy current density and then losses density are given by

$$J_r(r,z) = \frac{I}{2\pi r}\left[\frac{(1+j)q \cdot \sinh\left[(1+j)qz\right]}{\cosh\left[(1+j)qc/2\right]}\right] \tag{2.14}$$

$$\frac{|J_r|^2}{\sigma} = \frac{2}{\sigma}\left(\frac{Iq}{2\pi r}\right)^2\left[\frac{\cosh(2qz)-\cos(2qz)}{\cosh(qc)+\cos(qc)}\right] \tag{2.15}$$

In addition, considering only the radial component of eddy current density and neglecting the axial component due to its small value cover losses is given by relation (2.16) [16].

$$Loss_{bush} = \frac{I^2 q}{\pi\sigma}\ln\left(\frac{b}{a}\right)\cdot\left[\frac{\sinh(qc)-\sin(qc)}{\cosh(qc)+\cos(qc)}\right] \tag{2.16}$$

2.1.2. The cover plate of transformer

The power flux of electromagnetic waves in z-axis at any time t given by Poynting vector $\mathbf{S}(z,t) = \mathbf{E}(z,t) \times \mathbf{H}(z,t)$. The time averaged Poynting vector $\mathbf{S}_{ave}(z)$ equals to (2.17), considering the time harmonic electromagnetic field as $\mathbf{E}(z,t) = \mathrm{Re}\left(\mathbf{E}_s(z)e^{j\omega t}\right)$ and $\mathbf{H}(z,t) = \mathrm{Re}\left(\mathbf{H}_s(z)e^{j\omega t}\right)$ where ω is the angular frequency.

$$\mathbf{S}_{ave}(z) = (1/2)\mathrm{Re}\left[\mathbf{E}_s(z) \times \mathbf{H}_s^*(z)\right] \tag{2.17}$$

where $\mathbf{E}_s(z)$ and $\mathbf{H}_s(z)$ are the phasor forms of electric and magnetic fields and $\mathbf{H}_s^*$ is the complex conjugate of $\mathbf{H}_s$. Therefore, the losses density over a metallic surface is given by (2.18), as a result of Poynting's theorem

$$\mathbf{S}_{ave}(0) = \hat{k}\sqrt{\frac{\omega\mu}{8\sigma}}H_{ms}^2 \tag{2.18}$$

where, μ is the magnetic permeability, σ is the electrical conductivity of the material and H_{ms} is the peak of the magnetic field at any point (x, y) on the metallic surface in the Cartesian coordinate system [26].

Therefore, leakage losses P_s of the steel cover plate in time harmonic magnetic fields are given by (2.19) [30]

$$P_s = \sqrt{\frac{\omega\mu}{8\sigma}}\iint |H_{ms}(x,y)|^2 \, dxdy \tag{2.19}$$

where H_{ms}, the maximum of the magnetic field intensity on the surface of the plate, can be determined by equation (2.20), using RMS definition.

$$H_{ms}^2 = (2/T)\int_0^T h^2(t)dt \tag{2.20}$$

where, $h(t)$ is the instant magnetic field vector at a point in the around space of a given current distribution. The Biot-Savart law is used to determine $h(t)$. Therefore, the maximum magnetic field at any considered point (*x, y*) on the surface of the cover plate with one conductor is expressed by (2.21).

$$H_{ms}(x,y) = I_m \Big/ \left(2\pi\sqrt{x^2+y^2}\right) \tag{2.21}$$

The magnetic field *h* of a 3-phase current bushing in a typical point on the cover plate surface, as shown in Figure 2.5, is divided into its azimuthal and radial components $h^2 = h_\theta^2 + h_r^2$ at cylindrical coordinate system and then can be find out as follows:

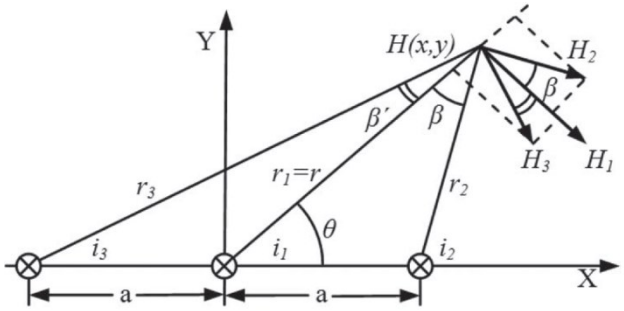

Figure 2.5. Magnetic field intensity calculation on 3-phase cover plate [22].

$$h^2 = \frac{1}{(4\pi)^2}\left\{\left(\frac{i_1}{r_1}+\frac{i_2\cos\beta}{r_2}+\frac{i_3\cos\beta'}{r_3}\right)^2+\left(\frac{i_2\sin\beta}{r_2}+\frac{i_3\sin\beta'}{r_3}\right)^2\right\} \text{ or}$$

$$h^2 = \frac{1}{(4\pi)^2}\left\{\left(\frac{i_1}{r_1}\right)^2+\left(\frac{i_2}{r_2}\right)^2+\left(\frac{i_3}{r_3}\right)^2+\frac{2i_1i_2\cos\beta}{r_1r_2}+\frac{2i_1i_3\cos\beta'}{r_1r_3}+\frac{2i_2i_3}{r_2r_3}\left(\cos\beta\cos\beta'-\sin\beta\sin\beta'\right)\right\}$$

where i_1, i_2 and i_3, 3-phase balanced currents, are defined as:

$$\begin{aligned} i_1 &= I_m sin(\omega t), \\ i_b &= I_m sin(\omega t - 2\pi/3), \\ i_c &= I_m sin(\omega t + 2\pi/3) \end{aligned} \tag{2.22}$$

Substituting h^2 into equation (2.20) and then integrating, the squared peak of the magnetic field can be given as

$$H_m^2 = \frac{1}{(4\pi)^2}\left\{\left(\frac{I_m}{r_1}\right)^2+\left(\frac{I_m}{r_2}\right)^2+\left(\frac{I_m}{r_3}\right)^2-\frac{I_m^2\cos\beta}{r_1r_2}-\frac{2I_m^2\cos\beta'}{r_1r_3}-\frac{I_m^2}{r_2r_3}\left(\cos\beta\cos\beta'-\sin\beta\sin\beta'\right)\right\}$$

after simplifying

$$H_m^2 = \left(\frac{I_m}{4\pi}\right)^2\frac{1}{(r_1r_2r_3)^2}\left\{\begin{array}{l}(r_2r_3)^2+(r_1r_3)^2+(r_1r_2)^2-r_1r_2r_3^2\cos\beta-r_1r_2^2r_3\cos\beta'- \\ r_1^2r_2r_3\cos\beta\cos\beta'+r_1^2r_2r_3\sin\beta\sin\beta'\end{array}\right\} \tag{2.23}$$

using the following mathematical relationships, obtained from Figure 2.5,

$r_1^2 = x^2 + y^2$,

$r_2^2 = (x-a)^2 + y^2 \Rightarrow r_2^2 - a^2 = r_1^2 - 2ax$,

$r_3^2 = (x+a)^2 + y^2 \Rightarrow r_3^2 - a^2 = r_1^2 + 2ax$,

$\cos\beta = \dfrac{r_1^2 + r_2^2 - a^2}{2r_1r_2} \Rightarrow r_1r_2\cos\beta = r_1^2 - ax$,

$$\cos\beta' = \frac{r_1^2 + r_3^2 - a^2}{2r_1 r_3} \Rightarrow r_1 r_3 \cos\beta' = r_1^2 + ax,$$

$$\sin\theta = \frac{y}{r_1},$$

$$\frac{\sin\beta}{a} = \frac{\sin\theta}{r_2},$$

$$\frac{\sin\beta'}{a} = \frac{\sin(\pi - \theta)}{r_3} = \frac{\sin\theta}{r_3}$$

the last four terms of equation (2.23) can be rewritten as follow, respectively:

$$-r_1 r_2 r_3^2 \cos\beta = -r_3^2\left(r_1^2 - ax\right),$$

$$-r_1 r_2^2 r_3 \cos\beta' = -r_2^2\left(r_1^2 + ax\right),$$

$$-r_1^2 r_2 r_3 \cos\beta\cos\beta' = -\left(r_1^2 - ax\right)\left(r_1^2 + ax\right) = -r_1^4 + (ax)^2,$$

$$r_2 r_3 \sin\beta\sin\beta' = r_2 r_3 \frac{a\sin\theta}{r_2}\frac{a\sin\theta}{r_3} = (a\sin\theta)^2 = \left(a\frac{y}{r_1}\right)^2 = \frac{(ay)^2}{r_1^2}$$

substituting the obtained relations into (2.23) leads to

$$H_m^2 = \left(\frac{I_m}{4\pi}\right)^2 \frac{1}{(r_1 r_2 r_3)^2}\left\{(r_2 r_3)^2 + axr_3^2 - axr_2^2 - r_1^4 + (ax)^2 + (ay)^2\right\},$$

substituting for the first four terms in a Cartesian coordinate system as follow,

$$(r_2 r_3)^2 = x^4 + y^4 + 2(xy)^2 - 2(ax)^2 + 2(ay)^2 + a^4,$$

$$axr_3^2 - axr_2^2 = 4(ax)^2,$$

$$-r_1^4 = -x^4 - 2(xy)^2 - y^4$$

the peak of the magnetic field of 3-phase balanced currents, in any point on the plate surface, can be obtained by (2.24).

$$H_{ms}(x,y) = \frac{I_m a}{2\pi}\sqrt{\frac{3\left(x^2 + y^2\right) + a^2}{\left(x^2 + y^2\right)\left(x^4 + y^4 + 2(xy)^2 - 2(ax)^2 + 2(ay)^2 + a^4\right)}} \qquad (2.24)$$

where, I_m is the peak value of current and a is the distance between the current conductors[22], [31].

As a result, the incident tangential field of the cover plate is directly proportional to the source current. Therefore, the power losses will be directly proportional to the squared current.

2.2. Thermal Analysis

The losses density $p_v(\mathbf{r})$ given by (2.9) at any position $\mathbf{r}$ obtained from magnetic solution of model is imported to the transient thermal analysis as heat sources.

$$\frac{\partial}{\partial x}\left(k\frac{\partial T}{\partial x}\right)+\frac{\partial}{\partial y}\left(k\frac{\partial T}{\partial y}\right)+\frac{\partial}{\partial z}\left(k\frac{\partial T}{\partial z}\right)=\rho C_p\frac{\partial T}{\partial t}-p_v \tag{2.25}$$

The heat conduction equation [32] of the cover plate (2.26) in a cylindrical coordinate system can be simplified to a parabolic PDE (2.26) because of axisymmetric behavior [33],

$$\rho C_p\frac{\partial T}{\partial t}=k\left[\left(\frac{1}{r}\frac{\partial T}{\partial r}+\frac{\partial^2 T}{\partial r^2}\right)+\frac{\partial^2 T}{\partial z^2}\right]+p_v \tag{2.26}$$

where k, ρ, C_p and T are thermal conductivity, density, specific heat and temperature of the cover steel, respectively.

Multiplying by r the equation (2.26) can be rewritten as:

$$\rho C_p r\frac{\partial T}{\partial t}-\frac{\partial}{\partial r}\left(kr\frac{\partial T}{\partial r}\right)-\frac{\partial}{\partial z}\left(kr\frac{\partial T}{\partial z}\right)=rp_v \tag{2.27}$$

Equation (2.27) can be converted into 2D form in Cartesian coordinate system if r is defined as x and z is defined as y. Therefore, equation (2.27) changes to (2.28).

$$\rho C_p x\frac{\partial T}{\partial t}-\nabla\cdot\left(kx\nabla T\right)=xp_v \tag{2.28}$$

In the transient solution case, the plate temperature can be determined as a function of time. The heat conduction equation in the steady-state condition is simplified as (2.29) [33].

$$-\frac{\partial}{\partial r}\left(kr\frac{\partial T}{\partial r}\right)-\frac{\partial}{\partial z}\left(kr\frac{\partial T}{\partial z}\right)=rp_v \tag{2.29}$$

At steady state solution, the final temperature of plate as a result of the equilibrium state can be observed.

Convection and radiation forms of heat transfer (2.30) have been chosen as thermal heat flux boundary at the cover surfaces,

$$q_{cr} = h_c\left(T - T_a\right) + \varepsilon_r \sigma_r \left(T^4 - T_a^4\right) \tag{2.30}$$

where h_c, ε_r, σ_r and T_a are the heat transfer coefficient, the emissivity coefficient, the Stefan–Boltzmann constant and the ambient temperature, respectively.

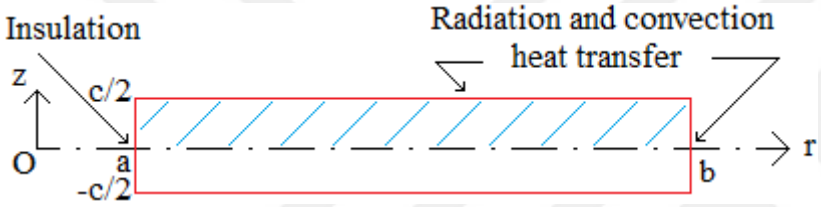

Figure 2.6. The thermal BCs of the cover plate

The applied thermal BCs on the surfaces of the cover as illustrated in Figure 2.6 are the heat balance equations between conduction heat transfer in the cover plate and convection and radiation heat transfer to the ambient (2.31) [15].

$$\hat{n} \cdot q_k = q_{cr} \tag{2.31}$$

where q_k , the conduction heat transfer, is given by:

$$q_k = -k\nabla T \tag{2.32}$$

where k is the thermal conductivity of the steel [15].
Substituting q_k, q_{cr} from (2.30) and (2.32) into (2.31) and rewriting it, yields

$$\hat{n} \cdot \left(k\nabla T\right) + \left(h_c + \varepsilon_r \sigma_r T^3\right) T = h_c T_a + \varepsilon_r \sigma_r T_a^4 \tag{2.33}$$

where $\hat{n}$ is the outward unit normal vector at a typical point.

Natural convection coefficient h_c of the horizontal plate in an ambient is computed using basic thermal theory. Rayleigh number is given by

$$Ra = Gr \cdot Pr \tag{2.34}$$

where Gr and Pr are dimensionless group called the Grashof and Prandtl numbers respectively, which are determined by

$$Gr = g\beta\Delta Tl^3\rho^2 / \mu^2 \tag{2.35}$$

and

$$Pr = \mu c_p / k \tag{2.36}$$

where μ, β, k and ρ are called the dynamic viscosity, fluid thermal expansion coefficient, thermal conductivity and density of the fluid respectively and determined at film temperature(the average temperature of the plate and air/oil) and l is the length parameter or characteristic dimension of the cover plate.

The Nusselt number for natural convection heat transfer of the upper surface heated plate is then calculated [32, 34] as (2.37),

$$\begin{aligned} &Nu = 0.54Ra^{1/4} \text{ valid for } 2\times10^4 < Ra < 8\times10^6 \\ &Nu = 0.15Ra^{1/3} \text{ valid for } 8\times10^6 < Ra < 10^{11} \end{aligned} \tag{2.37}$$

and for lower surface heated plate is determined as (2.38)

$$Nu = 0.27Ra^{1/4} \text{ valid for } 10^5 < Ra < 10^{11} \tag{2.38}$$

therefore, the convection coefficient is given by

$$h_c = Nuk/l \tag{2.39}$$

The characteristic dimension for a horizontal rectangle plate can be determined by

$$l = A / P \tag{2.40}$$

where has a better agreement with experimental data. For example, the characteristic dimension of the rectangle plate in Figure 5.1 with A = 1.5×0.7 m^2 area and P = 2×(1.5×0.7) m circumference becomes 0.24 m. In the case of the circular plate as depicted in Figure 2.1 the characteristic dimension l is calculated by $l = \pi r^2 / (2\pi r) = r/2 = b/2$.

3. FEM SOLUTION APPROACH

The FEM is a numerical technique for solving differential equations in many disciplines, e.g., electromagnetics, magneto-statics, thermal conduction. The core idea of the FEM is to approximate the overall complicated problem of solving the differential equations to a series of simpler sub-problems that corresponds to an easily solved linear system of equations. The sub-problems are described geometrically by geometrically simple shaped elements such as triangles for 2D and mainly tetrahedrons for 3D problems. These elements forming the numerical discretization, the mesh, are called the FEs. On this discretization, the problem-describing differential equation is locally approximated by a simple shape function. Assembling all sub-problems into a system of equations and solving this obtains an approached overall solution[35].

3.1. Magnetic Field and Eddy Losses FEM Approach

In general, the procedure for solving FEM electromagnetic field problem is divided into three steps:

1. Pre-processing: the electromagnetic field problem is defined and prepared to be solved, such as eddy losses density in a cover plate.
2. Processing: the numerical solution of the physical problem is obtained such as solution of the magnetic field in the cover plate.
3. Post-processing: the solution obtained is prepared to calculate the required electromagnetic field quantities such as eddy current and losses density in the cover plate.[35]

The 3D eddy current problem equations which is applied in the simulation of transformer cover plate using A and A-φ potential formulation as following

$$\nabla \times \frac{1}{\mu} \nabla \times A + \sigma \frac{\partial A}{\partial t} + \sigma \nabla \varphi = 0 \quad \text{in} \quad \Omega_1 \tag{3.1}$$

$$\nabla \times (1/\mu) \nabla \times A = J_s \quad \text{in} \quad \Omega_2 \tag{3.2}$$

which, Ω_1 and Ω_2 are eddy current and other regions respectively, A is the magnetic vector potential, φ is the electric scalar potential, J_s is a source current density. For a sinusoidal field variation $j\omega$ is substituted by $\partial/\partial t$ into Equation (3.1) [36-38].

ANSYS's Maxwell 3D is a high-performance interactive software package that uses FE analysis (FEA) to solve eddy current, and transient problems. One of the applications of the eddy current analysis can be stray field calculations. Eddy current analysis in Maxwell program is performed by choosing the Eddy Current or Transient solution type.

The Eddy Current solver computes steady state at a given frequency. The excitation source of the static magnetic field can be the peak of the sinusoidal AC current in the conductors. The RMS current of low voltage side in 3-phase transformers has been calculated by the following equation:

$$I = 1000 \times S \Big/ \left(\sqrt{3} V_{L-L} \right) \tag{3.3}$$

where S is the apparent power in kVA and $V_{L\text{-}L}$ is the line to line voltage of low voltage side of the transformer. Therefore, balanced 3-phase currents using (2.22) and (3.3) are given as

$$\begin{aligned} i_a &= \left(1 - exp\left(-t/T\right)\right) I\sqrt{2} sin\left(\omega t\right) \\ i_b &= \left(1 - exp\left(-t/T\right)\right) I\sqrt{2} sin\left(\omega t - 2\pi/3\right) \\ i_c &= \left(1 - exp\left(-t/T\right)\right) I\sqrt{2} sin\left(\omega t + 2\pi/3\right) \end{aligned} \tag{3.4}$$

where current peak exponentially increases up to the maximum to eliminate the overshoot peak of the step response in the transient solution of the losses. Consequently, the time to reach to steady state is decreased.

The Transient magnetic solver computes magnetic fields in the time domain. The source of the static magnetic field can be arbitrary time-varying current in conductors. Material permeability can be nonlinear and/or anisotropic.

The Eddy Current solver performs an adaptive mesh solution. This means that the FE mesh is intelligently improved from one adaptive pass to the next. But, the Transient solver does

not have an adaptive mesh solution, so significant, intelligent mesh operations are required. There are techniques to obtain more defined mesh, such as linking a Transient simulation to the mesh from an Eddy Current simulation. The skin depth based mesh operation is most important in any simulations where eddy currents and therefore losses are important to the solution of the simulation.

In the both solvers, the quantities solved are the magnetic field (H) and the magnetic scalar potential (φ). Current density (J), magnetic flux density (B) are then calculated from H by using (2.4). Therefore, eddy losses may be calculated by (2.9) from these basic field quantities [27].

3.2. Thermal FEM Approach

As discussed in the previous sections, the maximum temperature arise in the tank cover because of the induced stray losses. Therefore, the temperature rise of the cover can be estimated by coupling between the magnetic and thermal analyses whereas the stray losses density of the plate is taken into account as heat source.

In the FEM thermal analysis of the cover plate, the heat conduction equation (2.27) and the thermal boundary condition (2.30) are used. 3D FEM thermal analysis of the cover plate has been done in ANSYS program. PDE Toolbox of MATLAB is used to do 2D FEM thermal analysis near the bushing region of the cover plate.

PDE Toolbox™ of MATLAB provides functions for solving PDEs in 2D, 3D, and time using FE analysis. It is possible to specify and mesh 2D and 3D geometries and formulate boundary conditions and equations. It can be solved static, time domain, frequency domain, and eigenvalue problems over the domain of the geometry. Functions for post-processing and plotting results enables to visually explore the solution[39].

For the case of the cover with one conductor, the solution domain is 2D due to symmetry. Therefore, for 2D FEM thermal analysis of the problem, we have used equations (2.28) and (2.29) in the case of transient and steady state condition, respectively.

For 2D FEM thermal analysis of the cover plate with one conductor, we have applied equations (2.28) and (2.29) under the boundary condition (2.33) at transient and steady state condition, respectively.

So that, the temperature distribution of tank cover can be obtained by importing the eddy losses densities obtained from the magnetic FE analysis into the thermal FE analysis as heat sources [27].

4. FDM SOLUTION APPROACH IN BUSHING REGIONS

The solution of PDEs by means of FD is based on approximating derivatives of continuous functions, i.e. the actual PDE, by discretized versions of the derivatives based on discrete points of the functions of interest. FD approximations to PDEs can be derived through the usage of Taylor series expansions.

Considering the fact that FDM is more flexible to deal with the nonlinear constitutive law and easy-to-be implemented, the FDM is used to find an exact estimation of magnetic field and stray losses at a steel disk with accounting its non-linear behavior.

4.1. Transient FDM Approach

For 2D FD analysis, we need to divide the solution region into an equally spaced grid of nodes with different mesh in z and r-direction. The steel thickness will be replaced with a grid of nodes which is equal to 10 times of skin depth number of thickness [20]. Therefore, for our configuration (Table 5.1) a grid of 66 points for the z-axis should be sufficient. It is not necessary to save all the computations on grid nodes during the work time of solution.

FDM approximation of Equation (3.2) can be given by:

$$\begin{aligned}\sigma\left[B^{new}(i,j)-B(i,j)\right]/\Delta t = (1/r_i)\left[H(i+1,j)-H(i-1,j)\right]/(2\Delta r)+ \\ \left[H(i+1,j)-2H(i,j)+H(i-1,j)\right]/(\Delta r)^2 - \\ H(i,j)/r_i^2+\left[H(i,j+1)-2H(i,j)+H(i,j-1)\right]/(\Delta z)^2\end{aligned} \tag{4.1}$$

where $B(i,j)$ and $H(i,j)$ are the value of B and H on a grid node, $i=1,\cdots,N_r$, $j=1,\cdots,N_z$ for $N_r \times N_z$ point grid, $B^{new}(i,j)$ and $H^{new}(i,j)$ are the value of magnitude of magnetic flux density and magnetic field intensity at the next time step, respectively, $r_i = a+(i-1)\cdot\Delta r$ is the radial distance of mesh points, Δz and Δr are the distance between space points in z and r directions, Δt is the time step[40]. The magnetic field at every next time step can be obtained by simplifying (4.1).

$$B^{new}(i,j)=B(i,j)+\frac{\Delta t}{\sigma(\Delta r)^2}\begin{bmatrix}(1+\Delta r/2r_i)H(i+1,j)+\\(1-\Delta r/2r_i)H(i-1,j)-\\\left(2+(\Delta r/r_i)^2\right)H(i,j)\end{bmatrix}+\frac{\Delta t}{\sigma(\Delta z)^2}\begin{bmatrix}H(i,j+1)-\\2H(i,j)+\\H(i,j-1)\end{bmatrix} \tag{4.2}$$

Here, it should be noted that the following conditions for time step determination should be satisfied with (4.2) to achieve a stable converged solution.

$$\begin{aligned}&\Delta t\Big/\left(\sigma(\Delta z)^2\right)\le \mu_{r,diff}\mu_0/2\\&\Delta t\Big/\left(\sigma(\Delta r)^2\right)\le \mu_{r,diff}\mu_0/2\end{aligned} \tag{4.3}$$

where $\mu_{r,diff}$ is the relative differential permeability[41]. The time step size is determined by considering $\Delta z\le\Delta r$, due to small thickness and small penetration depth of steel cover.

$$\begin{aligned}&\Delta z\le\Delta r\Rightarrow\left(\mu_{r,diff}\mu_0/2\right)\sigma(\Delta z)^2\le\left(\mu_{r,diff}\mu_0/2\right)\sigma(\Delta r)^2\Rightarrow\\&\Delta t\le\left(\mu_{r,diff}\mu_0/2\right)\sigma(\Delta z)^2\end{aligned} \tag{4.4}$$

The time step may vary during process[20].

The surface boundary conditions at $j=1$, $j=N_z$ and all i are

$$H(i,j)=I_m\Big/\left(2\pi r_i\right)\sin(\omega t) \tag{4.5}$$

at $i=1$ and all j are

$$H(1,j)=I_m\Big/\left(2\pi a\right)\sin(\omega t) \tag{4.6}$$

at $i=N_r$ and all j are

$$H(N_r,j)=I_m\Big/\left(2\pi b\right)\sin(\omega t) \tag{4.7}$$

At starting time of the solution $t=0$, B and H values at all grid nodes are set to zero. At $t=\Delta t$, boundary values are set according to (4.5), (4.6) and (4.7). All the non-boundary values of $H(i,j)$ are still zero at this point. The new values of magnetic flux density, $B^{new}(i,j)$, can be calculated using Equation (4.2). $H^{new}(i,j)$ is given at all non-boundary nodes by the fitted function to the *B-H* curve. The solution algorithm usually continues for

about 6 periods of oscillation time of the bushing current. Thus, at new time interval of $t+\Delta t$, magnetic field intensity at boundary conditions $H(i,1)$, $H(i,N_z)$, $H(1,j)$ and $H(N_r,j)$ are derived according to (4.5), (4.6) and (4.7). The *H* values of other points changes from their initial values which is zero. Then, $B^{new}(i,j)$ are derived from (4.2) and the $H^{new}(i,j)$ for non-boundary points are determined using the fitted function to the *B-H* curve.

According to the fact that the time average eddy current losses can be found in the end of each cycle, the algorithm flowchart for eddy losses calculations terminates when the losses error between two successive cycles is less than a given tolerance.

The FD approximation of eddy current density (2.8) given by using the following approaches. For non-boundary nodes, a central difference approach defined as

$$\partial H_\varphi/\partial r=\left[H(i+1,j)-H(i-1,j)\right]/(2\Delta r) \tag{4.8}$$

$$\partial H_\varphi/\partial z=\left[H(i,j+1)-H(i,j-1)\right]/(2\Delta z) \tag{4.9}$$

For points on the $r=a$ surface where $i=1$ difference approach defined as [20]

$$\partial H_\varphi/\partial r=\left[-3H(1,j)+4H(2,j)-H(3,j)\right]/(2\Delta r) \tag{4.10}$$

At the other surface $r=a$ where $i=N_r$ difference approach defined as [20]

$$\partial H_\varphi/\partial r=\left[3H(N_r,j)-4H(N_r-1,j)+H(N_r-2,j)\right]/(2\Delta r) \tag{4.11}$$

For points on the surface $z=0$ where $j=1$ difference approach defined as

$$\partial H_\varphi/\partial z=\left[-3H(i,1)+4H(i,2)-H(i,3)\right]/(2\Delta z) \tag{4.12}$$

At the other surface where $j=N_z$ difference approach defined as

$$\partial H_\varphi/\partial z=\left[3H(i,N_z)-4H(i,N_z-1)+H(i,N_z-2)\right]/(2\Delta z) \tag{4.13}$$

Equations (4.10), (4.11), (4.12) and (4.13) are second order differential types used to satisfy the required accuracy [40].

The time average eddy current losses of steel plate over a period can be determined as

$$Loss_{bush} = \frac{2\pi}{T\sigma} \sum_{k=1}^{k=T_n} \Delta t \sum_{j=1}^{j=N_z} \Delta z \sum_{i=1}^{i=N_r} \left|\mathbf{J}(i,j,k)\right|^2 r\Delta r \tag{4.14}$$

where **J** is an instantaneous eddy current density at any points of grid and T is the cycle period.

Normally, the minimum value of differential permeability is given by using the peak of magnetic field intensity $I_m/2\pi a$ over a period from (4.6). Therefore, the time step can be defined according to (4.4). For some margin, the time step must be set lower [20].

For checking the proposed method, a linear calculation of the eddy current losses have been done.

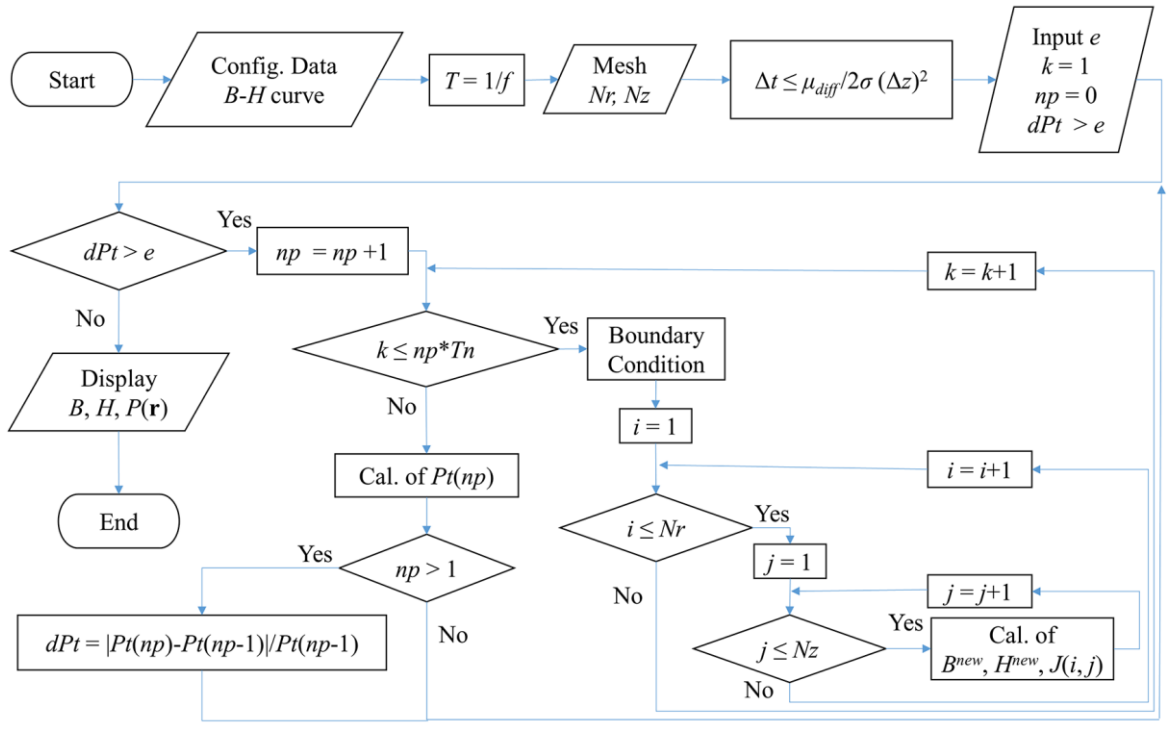

Figure 4.1. Flowchart corresponding to the proposed methodology for the stray losses calculation by FDM

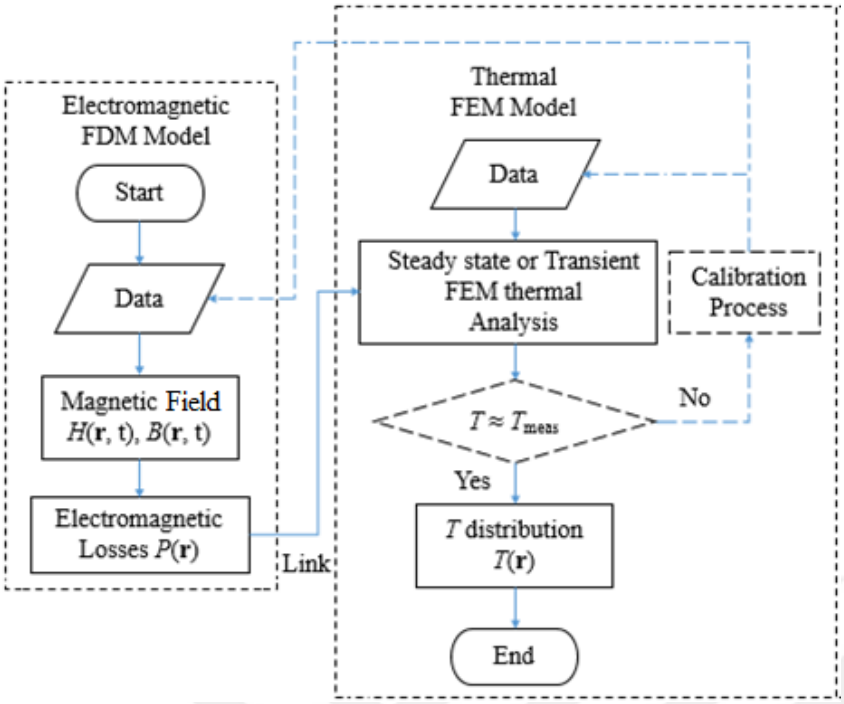

Figure 4.2. Flowchart corresponding to the proposed methodology for the electromagnetic and thermal link models

2D FD transient solution of the eddy losses has been done based on the algorithm in Figure 4.1 in a programming tool like, MATLAB. In this figure, *e* is the target tolerance of the eddy current losses between two successive period numbers, *np* is the number of period in which the calculations have been done and *Pt* is the eddy current losses at each period. The last period losses are imported into a steady state and transient thermal 2D FE model as heat sources. Transient and steady state 2D FEM thermal analysis have been developed and solved by the PDE Tools of MATLAB, based on equations (2.28) and (2.29) respectively, and it is possible to apply non-linear radiative and convective flux boundary condition (2.33) according to the technique used in [42].

Some required physical parameters (natural convection coefficient, thermal conductivity and electrical conductivity) in magnetic and thermal analysis can be defined by using the calibration process for non-linear permeability with a current (1000 A) (Figure 4.2). After calibration, FDM and FEM simulations are carried out for a different load current of 500 A.

4.2. Steady State Adaptive-FDM Magnetic Approach

For a precise analysis of the cover losses, the mesh size in the penetration depth regions must be improved. Therefore, a non-uniform computational stencil of the solution grid has been applied to FDM approximation of the magnetic field differential equation as shown in Figure 4.3. (a) Taylor-series expansions of the magnetic field intensity in *r* and *z*-direction centered at point (*r, z*) are given by following equations, where high order terms (H.O.T.) have been neglected.

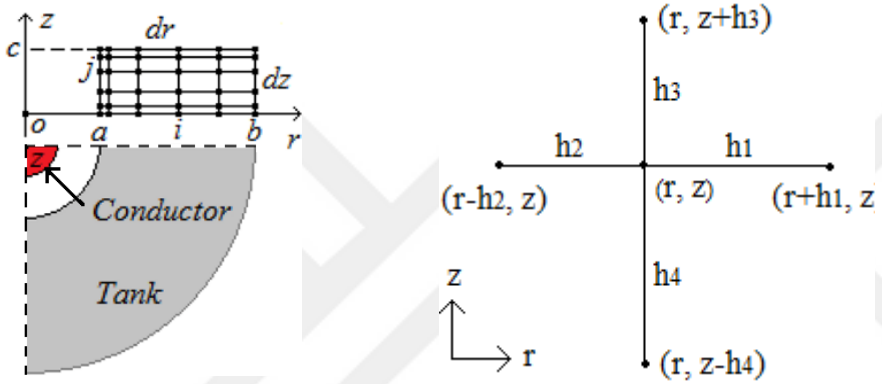

(a) (b)

Figure 4.3. (a) Idealized geometry and parameters used to calculate losses near the bushing region of a transformer cover by adaptive 2D FDM. (b) The computational stencil for the non-uniform FD scheme.

$$H(r+h_1,z)=H(r,z)+h_1\,\partial H/\partial r+\left(h_1^2/2\right)\partial^2 H/\partial r^2+...H.O.T. \tag{4.15}$$

$$H(r-h_2,z)=H(r,z)-h_2\,\partial H/\partial r+\left(h_2^2/2\right)\partial^2 H/\partial r^2-...H.O.T. \tag{4.16}$$

$$H(r,z+h_3)=H(r,z)+h_3\,\partial H/\partial z+\left(h_3^2/2\right)\partial^2 H/\partial z^2+...H.O.T. \tag{4.17}$$

$$H(r,z-h_4)=H(r,z)-h_4\,\partial H/\partial z+\left(h_4^2/2\right)\partial^2 H/\partial z^2-...H.O.T. \tag{4.18}$$

The FD approximation of the first derivatives at the points away from the boundaries are obtained as (4.19) and (4.20), namely central differences,

$$\begin{aligned}\partial H/\partial r&=\left[H(r+h_1,z)-H(r-h_2,z)\right]/(h_1+h_2)\\ \partial H/\partial z&=\left[H(r,z+h_3)-H(r,z-h_4)\right]/(h_3+h_4)\end{aligned} \tag{4.19}$$

$$\frac{\partial^2 H}{\partial r^2}=\frac{2}{h_1h_2}\left[\frac{h_2}{h_1+h_2}H\left(r+h_1,z\right)-H\left(r,z\right)+\frac{h_1}{h_1+h_2}H\left(r-h_2,z\right)\right]$$
$$\frac{\partial^2 H}{\partial z^2}=\frac{2}{h_3h_4}\left[\frac{h_4}{h_3+h_4}H\left(r,z+h_3\right)-H\left(r,z\right)+\frac{h_3}{h_3+h_4}H\left(r,z-h_4\right)\right] \quad (4.20)$$

We use one-sided second-order FD equations (4.21), (4.22) and (4.23) for improving the accuracy of the solution at boundary surfaces such as $r=a$, $r=b$ and $z=c/2$, respectively.

$$\frac{\partial H}{\partial r}=\frac{h_1+h_2}{h_1h_2}\left(H\left(r,z\right)-H\left(r-h_2,z\right)\right)+\frac{h_2}{h_1\left(h_1+h_2\right)}\left(H\left(r-h_2,z\right)-H\left(r+h_1,z\right)\right) \quad (4.21)$$

$$\frac{\partial H}{\partial r}=\frac{h_1+h_2}{h_1h_2}\left(H(r+h_1,z)-H(r,z)\right)+\frac{h_1}{h_2\left(h_1+h_2\right)}\left(H(r-h_2,z)-H(r+h_1,z)\right) \quad (4.22)$$

$$\frac{\partial H}{\partial z}=\frac{h_3+h_4}{h_3h_4}\left(H(r,z+h_3)-H(r,z)\right)+\frac{h_3}{h_4\left(h_3+h_4\right)}\left(H(r,z-h_4)-H(r,z+h_3)\right) \quad (4.23)$$

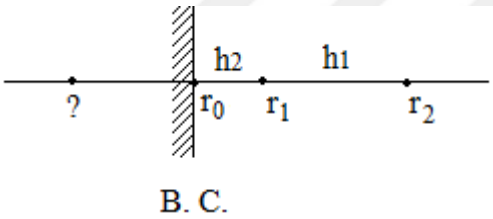

Figure 4.4. Illustration of boundary points in $r = a$ for one-sided FDs usage.

For obtaining one-sided FD approximation of the first derivatives or (4.21) at boundary surfaces such as $r=a$ considering its visualized model in Figure 4.4. Equation (4.15) simplified into (4.24) while ignoring high order terms.

$$H\left(r,z\right)=a+br+cr^2 \quad (4.24)$$

where $H\left(r,z\right)=H\left(0,z\right)+r\left(\partial H/\partial r\right)_0+\left(r^2/2\right)\left(\partial^2 H/\partial r^2\right)_0$, $a=H\left(0,z\right)=H_0$, $b=\left(\partial H/\partial r\right)_0$ and $c=(1/2)\left(\partial^2 H/\partial r^2\right)_0$. Rewriting (4.24) for points 1 and 2 according to Figure 4.4 we can have

$$H_1 = a + bh_2 + ch_2^2 \tag{4.25}$$

where $H_1 = H(h_2, z)$, and

$$H_2 = a + b(h_1 + h_2) + c(h_1 + h_2)^2 \tag{4.26}$$

where $H_2 = H(h_1 + h_2, z)$.

After eliminating c in equations (4.25) and (4.26), b or $(\partial H/\partial r)_0$ will be equal to (4.21) or $\frac{h_1 + h_2}{h_1 h_2}(H_1 - H_0) + \frac{h_2}{h_1(h_1 + h_2)}(H_0 - H_2)$.

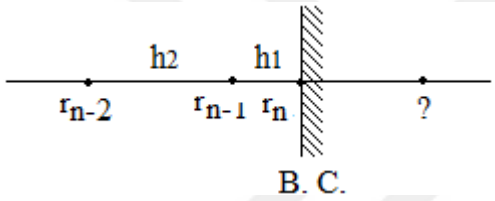

Figure 4.5.Illustration of boundary points in $r = b$ or $z = c/2$ for one-sided FDs usage.

Using the symmetry condition and invoking (4.21) in Figure 4.5 we can find equation $-\frac{h_1 + h_2}{h_1 h_2}(H_{n-1} - H_n) - \frac{h_1}{h_2(h_1 + h_2)}(H_n - H_{n-2})$ or (4.22) for one-sided FD in $r = b$ or $z = c/2$, where $H_n = H(0, z)$, $H_{n-1} = H(-h_1, z)$ and $H_{n-2} = H(-h_1 - h_2, z)$. In addition, invoking the uniform grid condition $h_1 = h_2 = \Delta r$ in (4.21) and (4.22) we can obtain equations (4.10) and (4.11), respectively.

Using non-uniform FD approximations of first and second-order of derivatives, the magnetic field differential equation (2.6) leads to a discrete model (4.27).

$$
\begin{aligned}
j\omega\sigma\mu H(r,z) &= (1/r)\left[H(r+h_1,z)-H(r-h_2,z)\right]/(h_1+h_2) \\
&\frac{2}{h_1h_2}\left[\frac{h_2}{h_1+h_2}H(r+h_1,z)-H(r,z)+\frac{h_1}{h_1+h_2}H(r-h_2,z)\right]+ \\
&\frac{2}{h_3h_4}\left[\frac{h_4}{h_3+h_4}H(r,z+h_3)-H(r,z)+\frac{h_3}{h_3+h_4}H(r,z-h_4)\right]
\end{aligned}
\tag{4.27}
$$

where h_1, h_2, h_3 and h_4 are the distance between a typical point and its neighbor points in r and z directions, respectively as seen in Figure 4.3. The simple and general form of the algebraic expression (4.27) for grid points is (4.28),

$$
\begin{aligned}
&A_{k,k-1}H(r,z-h_4)+A_{k,k-N_z}H(r-h_2,z)+\left(A_{k,k}-1/r^2\right)H(r,z)+ \\
&\qquad A_{k,k+N_z}H(r+h_1,z)+A_{k,k+1}H(r,z+h_3)=j\omega\sigma\mu H(r,z)
\end{aligned}
\tag{4.28}
$$

where the non-zero elements of A matrix in the k-th row are specified as following:

$$A_{k,k-1}=2/\left(h_4(h_3+h_4)\right) \tag{4.29}$$

$$A_{k,k-N_z}=(2/h_2-1/r)/(h_1+h_2) \tag{4.30}$$

$$A_{k,k}=-2\left(1/(h_1h_2)+1/(h_3h_4)\right) \tag{4.31}$$

$$A_{k,k+N_z}=(2/h_1+1/r)/(h_1+h_2) \tag{4.32}$$

$$A_{k,k+1}=2/\left(h_3(h_3+h_4)\right) \tag{4.33}$$

The Dirichlet BCs (as shown in Figure 2.2) at $r=a$, $r=b$ and $z=c/2$ surfaces are given by (4.34) which specify magnetic field intensity uniquely.

$$H(r,z) = I/(2\pi r) \tag{4.34}$$

For 2D FD analysis, we initially need to divide the solution region into an equally spaced grid of nodes with different mesh in z and r-direction. For our configuration (Table 5.1) an initial grid of 15 points for the z-axis and 60 point for r-axis is applied. Thus *B* and *H* fields are defined on a grid of points and their values are denoted as $B(i,j)$ and $H(i,j)$ respectively, where $i = 1,\cdots,N_r$, $j = 1,\cdots,N_z$ for an $N_r \times N_z$ point grid. Therefore, the general form of nonlinear system of equations (4.28) become as (4.35),

$$AH - b_1 H + b_2 = 0 \tag{4.35}$$

where, A is the known coefficients matrix of the equation, $H = \left[H(1) \cdots H(k) \cdots H(N_r N_z) \right]^T$ is a column matrix of unknown magnetic field intensities of the grid points, $b_1 = j\omega\sigma\mu$, for the linear magnetic permeability μ is a constant and for non-linear case μ equals to $B(H)/H$ is a function of *H* and $b_2(k) = A(k,j)H(k,j)$ are known at the boundary points.

The grid points order determined according to z-order curve. Z-order curve is a function which maps multidimensional data to one dimension while preserving locality of the data points.

For the adaptive mesh, the grids can be classified as *m*'s level based on the grid size. The *k*'s level grid size is defined as $\Delta l_k = \Delta l_0/(2k+1)$, $k \in [0,m]$, where Δl_0 is the maximal grid size for the zero's level mesh. The most simple AMR is to adopt the 2-level grids such as $(\Delta l_0, \Delta l_k)$, which can be easily coded in practice[43] and applied here as seen in Figure 4.6. The sophisticated AMR with multilevel grids has also been widely investigated in the literatures [44, 45]. The mesh points from left to right (or top to bottom) are the boundary, 2 level and initial points, respectively, where at the fine mesh, each FD region in the coarse mesh divided into 9 FDs. For the first level mesh, the solution of the non-linear system of equations (4.35) uses uniform initial mesh and the magnetic field Dirichlet BCs (Figure 2.2).

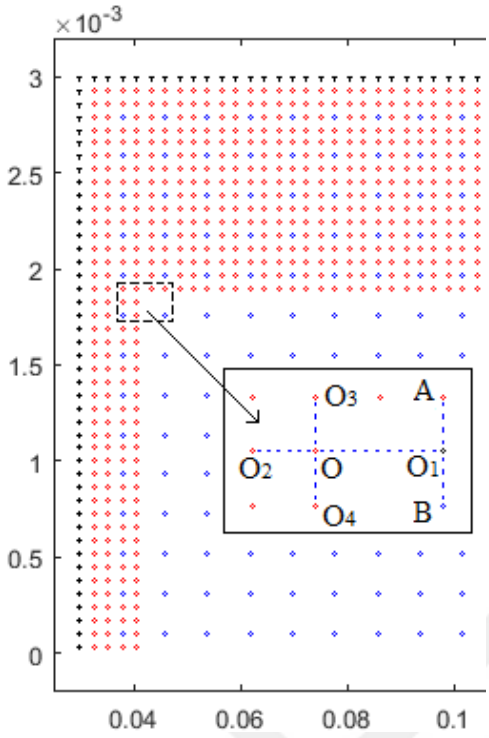

Figure 4.6. Illustration of 2-level local adaptive mesh.

For the grid near the interface between different level mesh, such as the grid O in two dimension depicted in Figure 4.6, five points (O, O_1, O_2, O_3, and O_4) are used to establish the second-order partial derivative of H for point O based on the equation (4.35). The intermediate value H_{O1} can be linearly interpolated from

$$H_{O1} = \left(H_A L_{BO_1} + H_B L_{AO_1}\right) \Big/ \left(L_{BO_1} + L_{AO_1}\right) \tag{4.36}$$

where L_{AO_1} is the distance between points A and O_1, L_{BO_1} is the distance between points B and O_1. The order of 2's sub steps is starting with the initial mesh and continuing with 2 level in the order of increasing resolution to improve the computational accuracy for the domains with large magnetic field gradients and high eddy currents. For the second level solution of equations (4.35) , we are using not only the old Dirichlet BCs but also new BCs, which defined by the first level solution results. As an example, the value of at point O is determined according to (4.36), where has been updated by the first level solution results. The non-linear system of magnetic field equations (4.35) in the two levels are solved by trust-region-dogleg algorithm. The dog-leg method finds a compromise between steepest descent step and Newton's step based on the size of the trust region [28, 29, 46].

At the magnetic steady state analysis, we are interested in obtaining the equilibrium state of magnetic field and then the losses density. The eddy current density in the solution region and boundary points is defined after replacing the derivatives in (2.8) with their non-uniform FD approximations given by (4.19), (4.21), (4.22) and (4.23) the non-uniform FD approach of (2.11) can be determined. Therefore, the plate losses can be calculated from

$$Loss = 2(2\pi/\sigma)\sum_{k}\left|\mathbf{J}(k)\right|^2 r_k \Delta r_k \Delta z_k \tag{4.37}$$

where k is the index of any point of solution grid, the constant coefficient 2 shows the symmetry condition.

4.3. ADI-FDM Thermal Approach

The losses density $p_v(\mathbf{r})$ at any position **r**, imported from adaptive FD magnetic analysis. FD approach of the thermal PDE of the plate (2.26) is given by equation (4.38). According to that, we need to divide the solution region into an equally spaced grid of nodes with different mesh in r and z-direction.

$$\frac{T^{new}(i,j)-T(i,j)}{\Delta t/2} = \frac{k}{\rho C_p}\left[\begin{array}{l}\dfrac{1}{r_i}\cdot\dfrac{T(i+1,j)-T(i-1,j)}{2\Delta r}+\\ \dfrac{T(i+1,j)-2T(i,j)+T(i-1,j)}{(\Delta r)^2}\end{array}\right]+ \\ \frac{k}{\rho C_p}\frac{T(i,j+1)-2T(i,j)+T(i,j-1)}{(\Delta z)^2}+\frac{p(i,j)}{\rho C_p} \tag{4.38}$$

where $T(i,j)$ is the determined value of temperature T in a grid node, $i=1,\cdots,N_r$, $j=1,\cdots,N_z$ for $N_r \times N_z$ grid points and $T^{new}(i,j)$ is shown the temperature value at the next time step.

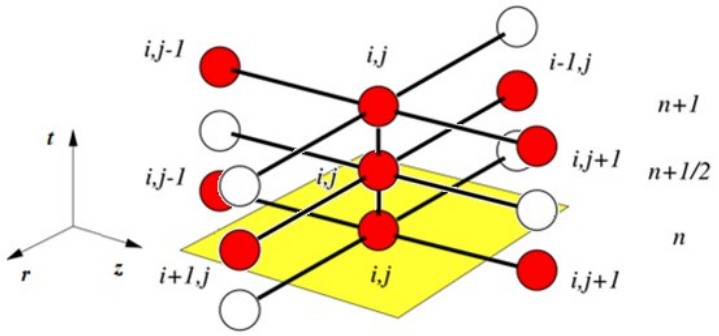

Figure 4.7. Stencil figure for the ADI method in FD equations [47].

An efficient numerical scheme for solving the parabolic PDE of heat conduction can be developed by ADI-FDM because it is fast in comparison with other methods (Explicit, Implicit and Crank-Nicolson schemes). In ADI method for 2D analysis, instead of advancing both directions in one step n+1, the r directions are advanced in a first implicit step of n+1/2 (as seen in Figure 4.7),

$$\frac{2}{\Delta t}T^{n+\frac{1}{2}}(i,j)-\frac{2}{\Delta t}T^{n}(i,j)=r_r\begin{bmatrix}\omega_i\left(T^{n+1/2}(i+1,j)-T^{n+1/2}(i-1,j)\right)+\\ T^{n+1/2}(i+1,j)-2T^{n+1/2}(i,j)+T^{n+1/2}(i-1,j)\end{bmatrix}+ \\ r_z\left[T^{n}(i,j+1)-2T^{n}(i,j)+T^{n}(i,j-1)\right]+\frac{p(i,j)}{\rho C_p} \tag{4.39}$$

and then the new z directions are found in a second implicit step of n+1

$$\frac{2}{\Delta t}T^{n+1}(i,j)-\frac{2}{\Delta t}T^{n+\frac{1}{2}}(i,j)=r_r\begin{bmatrix}\omega_i\left(T^{n+1/2}(i+1,j)-T^{n+1/2}(i-1,j)\right)+\\ T^{n+1/2}(i+1,j)-2T^{n+1/2}(i,j)+T^{n+1/2}(i-1,j)\end{bmatrix}+ \\ r_z\left[T^{n+1}(i,j+1)-2T^{n+1}(i,j)+T^{n+1}(i,j-1)\right]+\frac{p(i,j)}{\rho C_p} \tag{4.40}$$

where $\omega_i=\dfrac{\Delta r}{2r_i}$, $r_r=\dfrac{k}{\rho C_p(\Delta r)^2}$, $r_z=\dfrac{k}{\rho C_p(\Delta z)^2}$.

The simplified form of equations (4.39) and (4.40) can be derived as follow:

$$r_r(\omega_i-1)T^{n+1/2}(i-1,j)+\left(2r_r+\frac{2}{\Delta t}\right)T^{n+1/2}(i,j)-r_r(\omega_i+1)T^{n+1/2}(i+1,j)=b^n(i,j) \tag{4.41}$$

where $b^n(i,j)$ is a function of temperature at the pervious time step *n*.

$$b^n(i,j)=\frac{2}{\Delta t}T^n(i,j)+r_z\left[T^n(i,j+1)-2T^n(i,j)+T^n(i,j-1)\right]+\frac{p(i,j)}{\rho C_p} \tag{4.42}$$

and

$$r_z T^{n+1}(i,j-1)-(2r_z+2/\Delta t)T^{n+1}(i,j)+r_z T^{n+1}(i,j+1)=b^{n+1/2}(i,j) \tag{4.43}$$

where $b^{n+1/2}(i,j)$ is a function of temperature at the implicit step *n*+1/2.

$$\begin{aligned} b^{n+1/2}(i,j)=&-\frac{2}{\Delta t}T^{n+1/2}(i,j)-\frac{p(i,j)}{\rho C_p}- \\ &r_r\left[\omega_i\left(T^{n+1/2}(i+1,j)-T^{n+1/2}(i-1,j)\right)+T^{n+1/2}(i+1,j)-2T^{n+1/2}(i,j)+T^{n+1/2}(i-1,j)\right] \end{aligned} \tag{4.44}$$

The virtual grid points in the ADI-FDM equations, like $T(0,j)$, $T(N_r+1,j)$, $T(i,0)$, and $T(i,N_z+1)$, can be eliminated by using thermal BCs in the surfaces of $r=a$, $r=b$, $z=-c/2$ and $z=c/2$ (corresponding to indices of $i=1$, $i=N_r$, $j=1$ and $j=N_z$, respectively) as follow:

$$T(0,j)=T(2,j) \tag{4.45}$$

$$T(N_r+1,j)=T(N_r-1,j)-\frac{2\Delta r}{k}\left[h_c\left(T(N_r,j)-T_a\right)+\varepsilon_r\sigma_r\left(\left[T(N_r,j)\right]^4-T_a^4\right)\right] \tag{4.46}$$

$$T(i,0)=T(i,2)-\frac{2\Delta z}{k}\left[h_c\left(T(i,1)-T_a\right)+\varepsilon_r\sigma_r\left(\left[T(i,1)\right]^4-T_a^4\right)\right] \tag{4.47}$$

$$T(i,N_z+1)=T(i,N_z-1)-\frac{2\Delta z}{k}\left[h_c\left(T(i,N_z)-T_a\right)+\varepsilon_r\sigma_r\left(\left[T(i,N_z)\right]^4-T_a^4\right)\right] \tag{4.48}$$

For example, a proof of (4.46) according to Figure 2.6 is given by substituting $q_k = -k\left(\frac{\partial T}{\partial r}\hat{r} + \frac{\partial T}{\partial z}\hat{k}\right)$ and $\hat{n} = \hat{r}$ into (2.31), where $\hat{r}$ and $\hat{k}$ are unit vectors in the directions of *r* and z axes, respectively, leads to

$$-k\,\partial T/\partial r\big|_{r=b} = q_{cr}\big|_{r=b} \tag{4.49}$$

substituting q_{cr} from (2.30) into (4.49)

$$-k\,\partial T/\partial r\big|_{r=b} = \left\{h_c\left(T - T_a\right) + \varepsilon_r\sigma_r\left(T^4 - T_a^4\right)\right\}\Big|_{r=b} \tag{4.50}$$

therefore, the FD approximation of (4.50) will be (4.46).

Using source term linearization method [48], it is possible to apply linear approaches instead of the non-linear terms in (4.46), (4.47) and (4.48) at radiation parts. According to this method $q_r = q_r^* + \left(\partial q_r/\partial T\right)^*\left(T - T^*\right)$ is a linear approximation of $q_r = \varepsilon_r\sigma_r\left(T^4 - T_a^4\right)$ leads to

$$q_r = \varepsilon_r\sigma_r\left(\left(T^*\right)^4 - T_a^4\right) + \left(4\varepsilon_r\sigma_r\left(T^*\right)^3\right)\left(T - T^*\right) = 4\varepsilon_r\sigma_r\left(T^*\right)^3 T - 3\varepsilon_r\sigma_r\left(T^*\right)^4 - \varepsilon_r\sigma_r T_a^4 \tag{4.51}$$

where star(*) shows the old magnitude of the quantity. So that, the linear approach of q_{cr} becomes

$$q_{cr} = \left(h_c + 4\varepsilon_r\sigma_r\left(T^*\right)^3\right)T - \varepsilon_r\sigma_r\left(3\left(T^*\right)^4 + T_a^4\right) - h_c T_a \tag{4.52}$$

Therefore, the FD approximation of the linear estimation of BCs on the surfaces of $r = b$, $z = -c/2$ and $z = c/2$ are given by (4.53), (4.54) and (4.55) equations, respectively.

$$T^{n+\frac{1}{2}}\left(N_r + 1, j\right) = T^{n+\frac{1}{2}}\left(N_r - 1, j\right) - \frac{2\Delta r}{k}\left[\begin{array}{l}\left(h_c + 4\varepsilon_r\sigma_r\left(T^n\left(N_r, j\right)\right)^3\right)T^{n+1/2}\left(N_r, j\right) - \\ \varepsilon_r\sigma_r\left(3\left(T^n\left(N_r, j\right)\right)^4 + T_a^4\right) - h_c T_a\end{array}\right] \tag{4.53}$$

$$T^{n+1}(i,0)=T^{n+1}(i,2)-\frac{2\Delta z}{k}\left[\begin{array}{l}\left(h_c+4\varepsilon_r\sigma_r\left(T^{n+1/2}(i,1)\right)^3\right)T^{n+1}(i,1)-\\ \varepsilon_r\sigma_r\left(3\left(T^{n+1/2}(i,1)\right)^4+T_a^4\right)-h_cT_a\end{array}\right] \tag{4.54}$$

$$T^{n+1}(i,N_z+1)=T^{n+1}(i,N_z-1)-\frac{2\Delta z}{k}\left[\begin{array}{l}\left(h_c+4\varepsilon_r\sigma_r\left(T^{n+1/2}(i,N_z)\right)^3\right)T^{n+1}(i,N_z)-\\ \varepsilon_r\sigma_r\left(3\left(T^{n+1/2}(i,N_z)\right)^4+T_a^4\right)-h_cT_a\end{array}\right] \tag{4.55}$$

Considering the linear approaches, the virtual grid points of (4.41) and (4.42) have been eliminated by using (4.45), (4.53), (4.47) and (4.48) , respectively, and the virtual grid points of (4.43) and (4.44) have been eliminated by using (4.54), (4.55), (4.45) and (4.46), respectively.

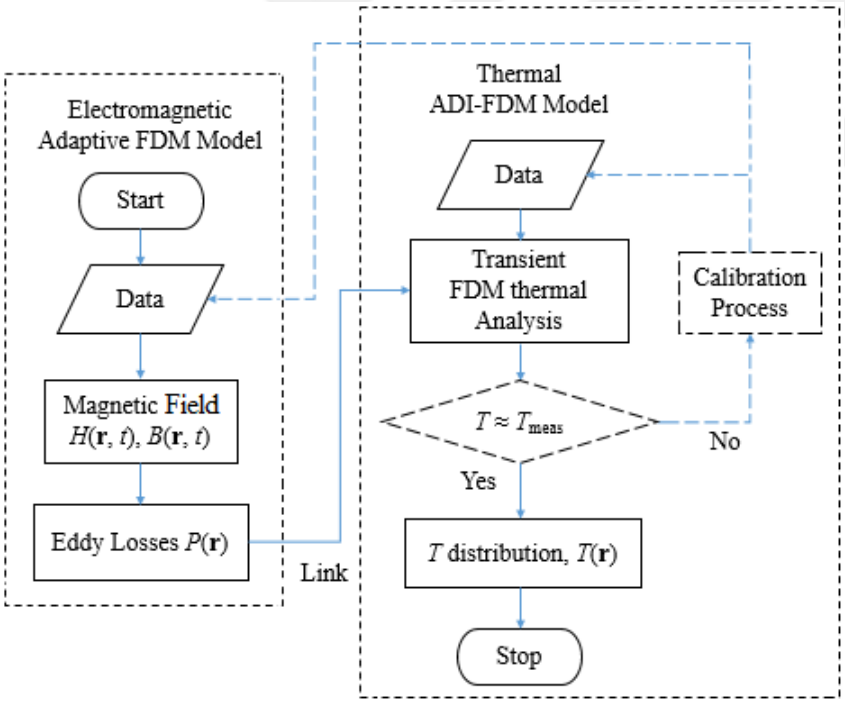

Figure 4.8. Calibration flowchart of the FDM magneto-thermal link models

In the transient analysis, we are interested in obtaining both the hot spot temperature of the cover as a function of time and the plate temperature distribution at the steady state condition.

The transient solution of the temperature distribution of cover model is computed based on the ADI-FD algorithm in a programming tool like MATLAB [49]. The heat source of this

model are the losses density obtained from a non-linear FD steady state solution. The required physical parameters in losses and thermal model are identified by means of a calibration process (Figure 4.8) in the case of 500 A current. After calibrating, simulation results are also carried out for a different load current of 1 000 A as shown in Figure 5.57.

5. THE RESULTS OF ANALYTICAL AND NUMERICAL SOLUTION APPROACHES

5.1. Case Studies

5.1.1. A disk plate as the bushing region of transformers cover

To validate the proposed methodology a disk (as seen in Figure 2.1) with the physical properties given in Table 5.1 has been taken into account. The copper conductor that crosses the disk has a radius of r = 24mm, a length of 1m, a relative magnetic permeability of $\mu_r = 1$ and an electrical conductance of σ = 58×106 Sm-1. The conductor current is 500 and 1000 A at 50 Hz.

The non-linear transient solution of the magnetic field can be done by applying *B-H* curve of the cover steel at each time interval of algorithm. The cover steel considered in this study has the magnetization curve of steel 1010 taken from material library of ANSYS's [27]. The relative permeability of 900 has been assumed in the case of linear analysis. The linear interpolation fitting method existing in mathematical library of MATLAB program is used in deriving the *B-H* curve.

Ambient temperature is assumed to have a value of 21.8°C. Parameter values used in this work have been taken from [19, 22] and after calibration process reproduced in Table 5.1.

Table 5.1. The geometry and physical properties of the disk steel ([19, 22])

Parameter	Symbol	Value
Hole radius	a	30mm
Disk radius	b	50cm
Disk thickness	c	6mm
Ambient Temperature	T_a	21.8°C
Steel relative permeability	μ_r	*B-H* curve (Figure 2.3)
Steel electrical conductivity	σ	6.8×10^6 Sm^{-1}
Emissivity coefficient	ε	0.23
Steel thermal conductivity	k	52 $Wm^{-1}K^{-1}$
Heat transfer coefficient	h_c	5 $Wm^{-2}K^{-1}$

5.1.2. The tank cover plate of transformer

The basic dimensions of 3-phase cover plate given in Figure 5.1 can be varied in the terms of three parameters of the non-magnetic slits wide, *B*, the distance *A* between the bushings and the diameter *D* of the bushing holes. For different values of conductor current of power transformer, the distance *A* between the bushings is 250 mm and the diameter *D* of the bushing holes is 70 mm according to [10] and in the case of distribution transformers their values given in Table 5.4.

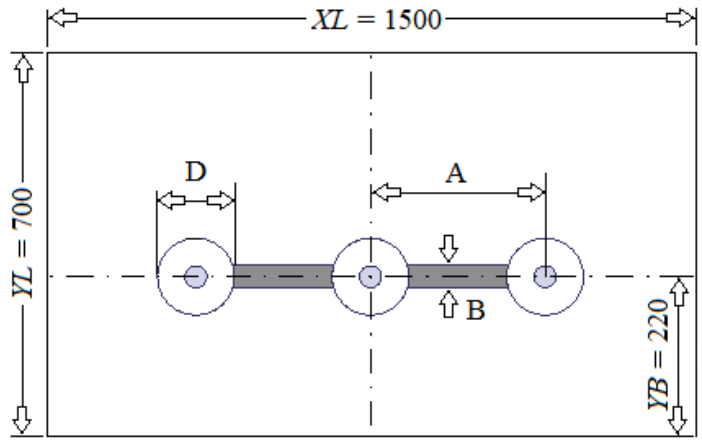

Figure 5.1. Computation model of transformer cover (Dimensions in mm).

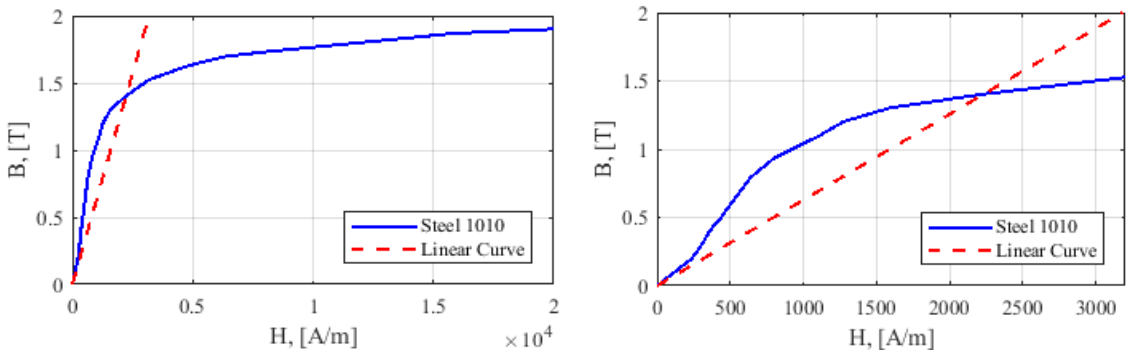

Figure 5.2. (a) *B-H* curve for steel 1010 compared with a linear curve (μ_r=500) and (b) Zoom-in into small magnetic fields to show detail changes.

The thickness of this computation model is 7.5 mm. The cover steel has relative permeability of 500 for linear case and a nonlinear permeability (Figure 5.2) for non-linear case and electric conductivity of 6.8×10^6 [S/m]. The non-magnetic SSI has a relative permeability of

1 and an electric conductivity of 1.1×10^{6} [S/m]. The copper conductors of bushing current has a relative permeability of 1, radius of 10 mm and electric conductivity of 58×10^{6} [S/m] [10].

5.2. Linear Magnetic Analytical Solutions

Linear magnetic analytic solution of the cover plate has been used here. The linear magnetic FD/FE analysis of the tank cover will be studied in the next sections.

In the first section, analytic solutions at bushing regions of the transformers cover have been investigated. In the second one, magnetic analytical solutions of the tank cover of 3-phase transformers have been proposed.

5.2.1. Bushing regions of the transformer cover

Considering case study of the bushing region, analytical magnetic field intensity and eddy current losses calculation results at steady state based on equations (2.12) and (2.15) have been given in Figure 5.3 and Figure 5.4, respectively, where the calculation domain has the mesh of $N_z = 60$ and $N_r = 300$ points in *z* and *r*-direction, respectively.

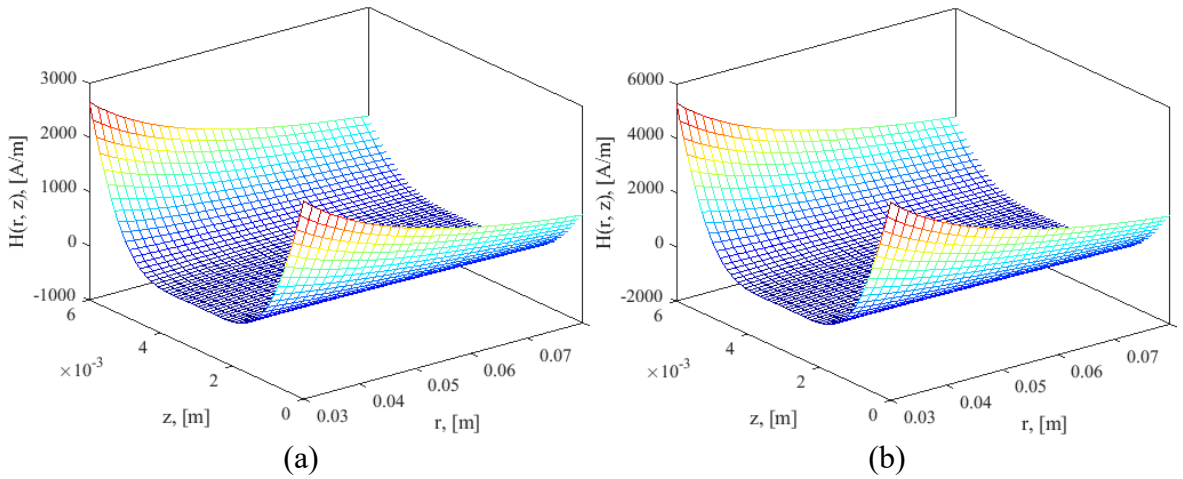

(a) (b)

Figure 5.3. Waveforms of magnetic field intensity at steady state conditions: (a) 500A, (b) 1 000 A.

As an approximation, in the case of losses density calculation, axial component of eddy current density has been ignored due to small values.

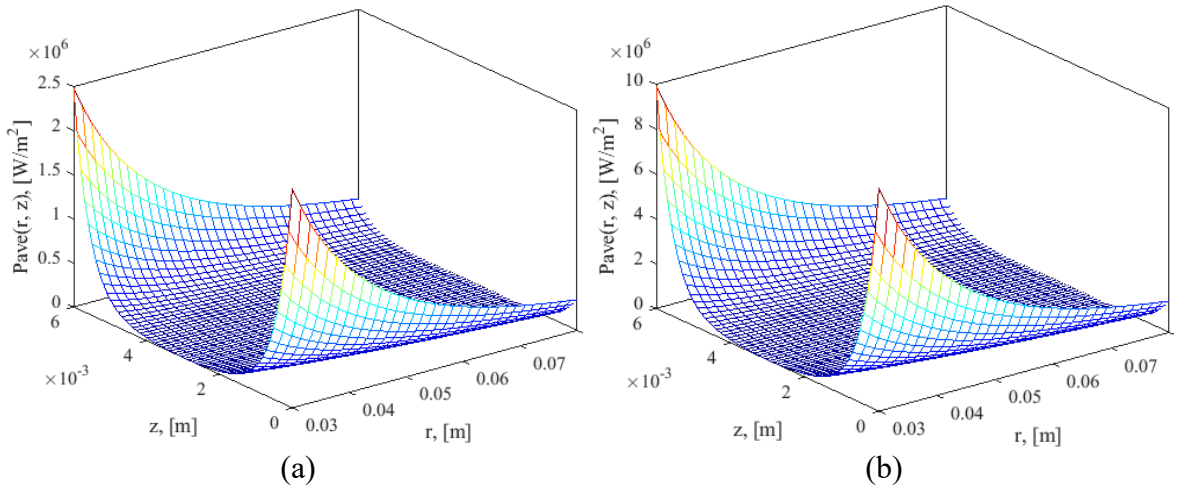

Figure 5.4. Waveforms of eddy losses distribution at steady state conditions: (a) 500A (b) 1000 A.

Table 5.2. Linear AM eddy current losses, [W] of the steel disk

Current, [A]	Linear Analytic , P_{total}
500	36.06
1 000	144.3

5.2.2. The cover plate of transformer

This study proposed a 3D FEM optimization design of cover plates for a 1 600 kVA, 400V 3-phase distribution transformer with a suitable geometry of SSI to overcome the local overheating and to keep the temperature below 140 °C. The stray magnetic field losses and hot spot temperature are estimated in the both cases of with and without SSI.

Figure 5.5 and Figure 5.6 demonstrate the MATLAB [49] outcomes of analytical calculations of maximum magnetic field and stray losses density over the cover plate of the 1 600 kVA, 400V, 50Hz 3-phase distribution transformer using Equations (2.19) and (2.24) respectively, in the 3D and 2D views. As a result, the maximum strength of the magnetic field and most of the losses are in the bushing regions and their between. It means this is the most important region, which must take into account in the optimal design procedure of cover plate.

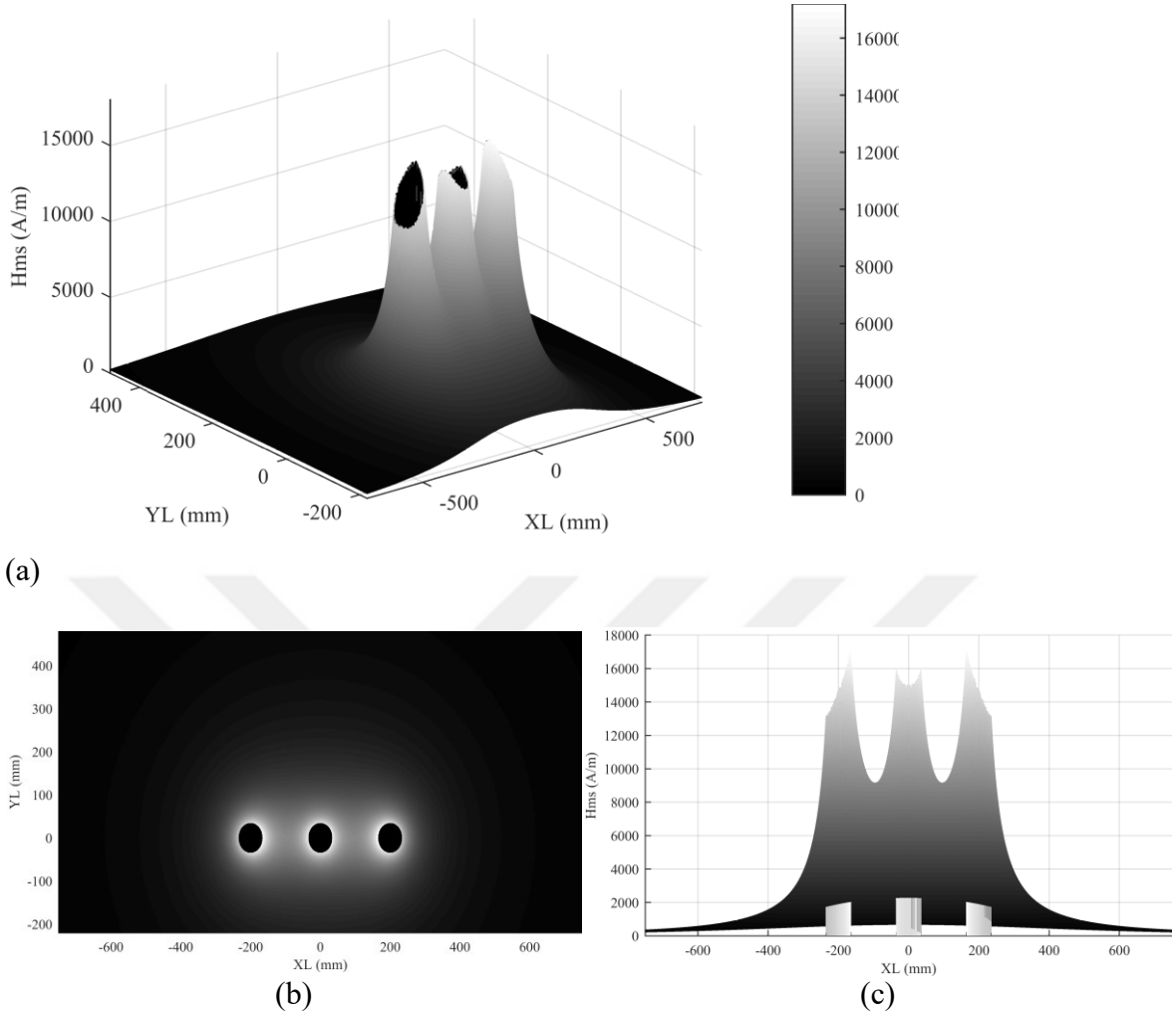

Figure 5.5. Analytical calculation of maximum magnetic field intensity of cover plate of a 1 600 kVA, 400 V 3-phase distribution transformer without SSI: (a) 3D display, (b), (c) 2D display

Table 5.3. The measured and analytical calculated stray losses in tank cover

I (A)	Measured Losses [10] (W)	Analytical Cal. Losses (W)	Error, [%]
1 000	246	247	0.4
1 500	487	555	13.96
2 000	917	987	7.63
2 500	1 442	1 542	6.93

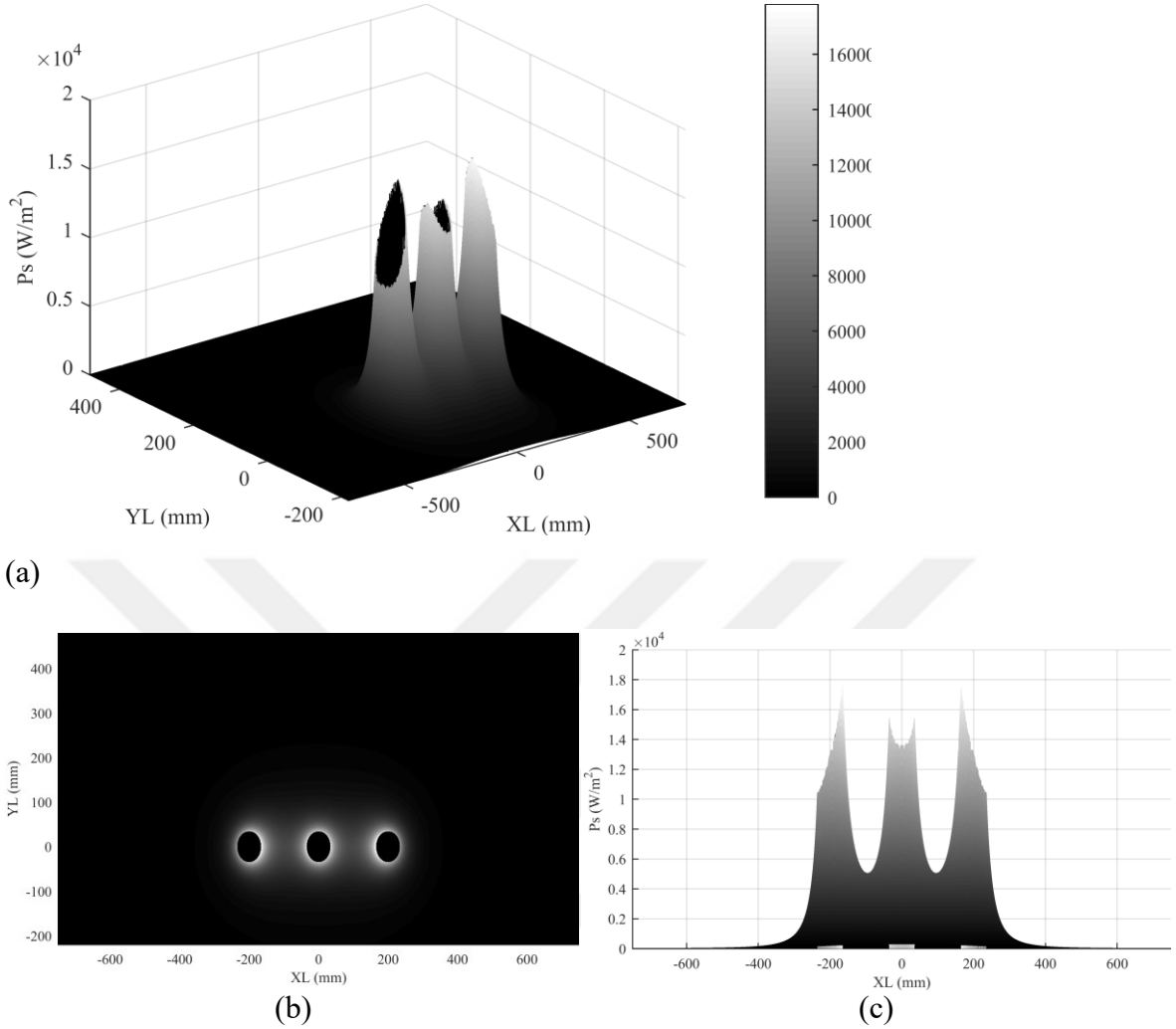

Figure 5.6. Analytical calculation of stray losses density of cover plate of a 1 600 kVA, 400V 3-phase distribution transformer without SSI: (a) 3D display, (b), (c) 2D display

Table 5.4. Analytical calculated stray losses in tank cover of 3-phase distribution transformers

S (kVA)	I (A)	A (mm)	D (mm)	Analytical Stray Loss Cal. (W)
630	909	150	55	190
800	1 155	150	55	307
1 000	1 443	150	55	479
1 250	1 804	200	70	725
1 600	2 309	200	70	1 233

5.3. Magneto-Thermal FE Analysis

In this section, the electromagnetic and thermal FE analysis of transformer cover plate have been done in a commercial FEM program namely ANSYS[27], according to a flow chart diagram shown in Figure 5.7. Time-harmonic eddy current solution of the model has been done under an adaptive mesh and using a linear or constant magnetic permeability. Non-linear magnetic FE analysis of the cover plate has been done by transient solution type of the program using an initial or imported mesh. Therefore, a non-linear adaptive FEM solution of the magnetic problem can be given by importing adaptive mesh from the time-harmonic solution. Then the eddy losses density of the steady-state electromagnetic solution are imported into the thermal analysis of the model.

In the first section, bushing regions of the transformers cover has been studied. In next section the tank cover of 3-phase transformers has been investigated considering the penetration depth of electromagnetic waves. In the last one, a fast calculation of hot spot temperatures of tank cover of 3-phase transformers has been proposed using surface impedance boundary condition of the cover steel.

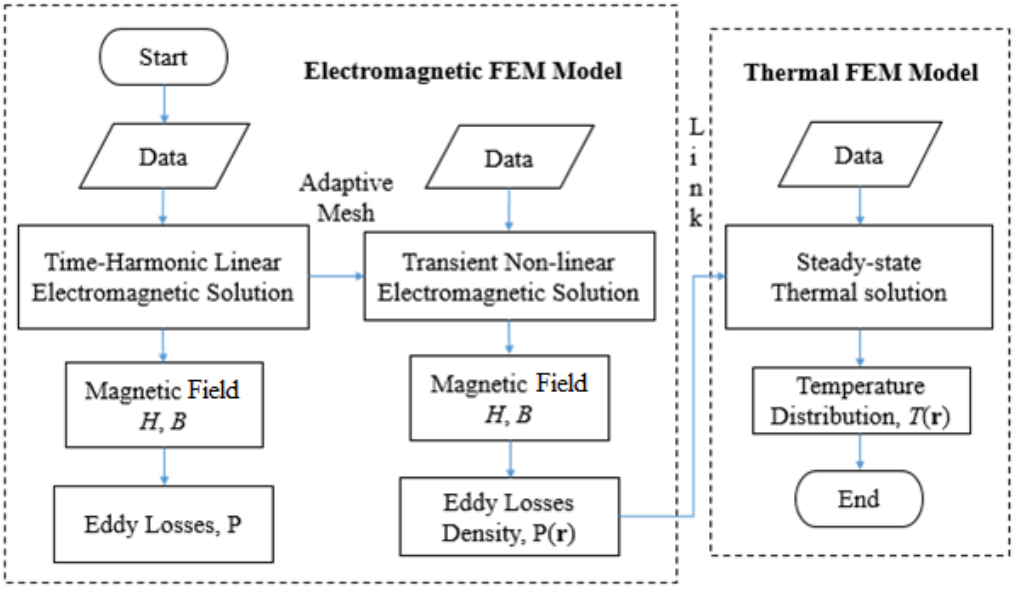

Figure 5.7. Flowchart of the magneto-thermal FE analysis

5.3.1. Bushing regions of the transformer cover

At the FEM model of the disk cover, we use only 1/720 of the disk, because of axial and azimuthal symmetries, to improve the computational cost. The flux BCs of the model have been given in Figure 5.8.

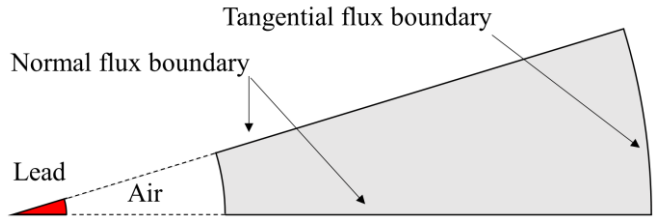

Figure 5.8. Flux boundary condition of the tank cover model.

Linear electromagnetic FE steady state analysis

Time-harmonic solution of the model has been done at 50Hz by eddy current solver.

An adaptive mesh with 36 700 FEs has been used in the FEM model of the tank cover as shown in Figure 5.9. For accurately estimating of the magnetic field and eddy losses in the depth of penetration, we use four FE layers with a thickness of 0.227 mm each in the skin depth of the disk, which it is equal to 0.91 mm.

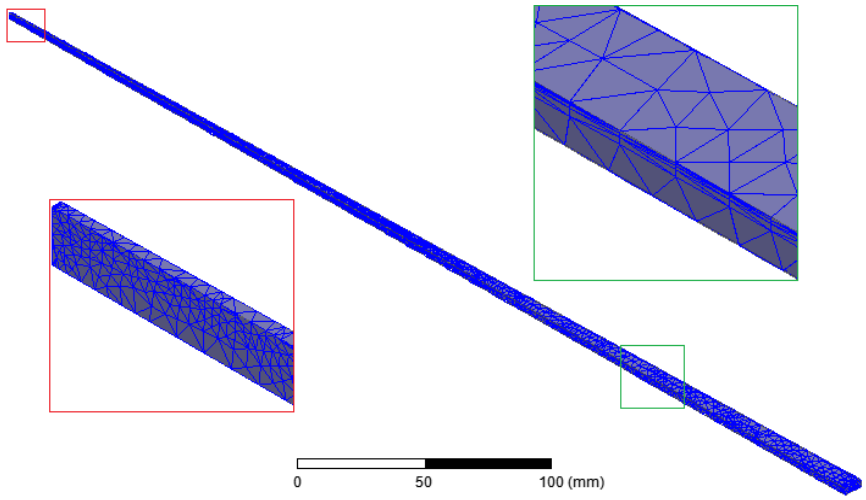

Figure 5.9. The total number of 36 700 adaptive FEs has been used in the cover plate model.

considering linear magnetic permeability of the steel plate. These have been performed to analyze magnetic field and stray losses in transformer cover plate at the both cases of without SSI and with SSI.

To calculate accurately the stray losses in the penetration depth of the cover plate, it is sufficient to consider fine mesh in the skin depth of the disk, 1.2mm, by setting two layers of 0.6 mm each, both on the top and bottom surfaces. In the case of this study, it is not necessary to consider the same fine mesh in SSI material because of bigger skin depth number, 67.9 mm, in comparison with plate thickness (7.5 mm). Therefore, the FE mesh number in the case of with and without SSI is approximately the same. The total number of 150 000 FEs is used in the simulated model as seen in Figure 5.19.

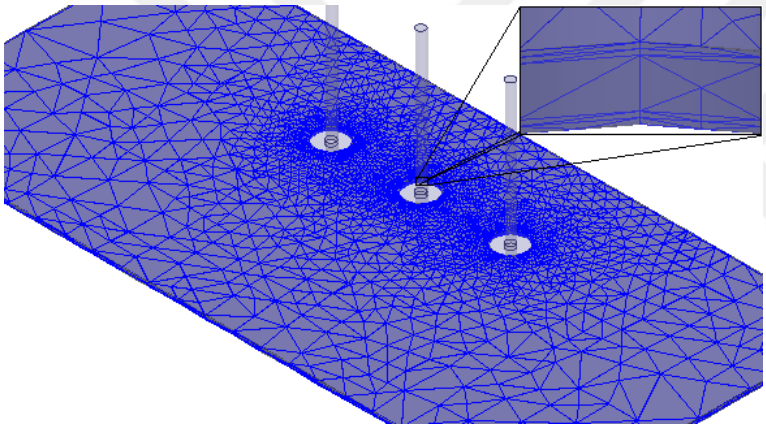

Figure 5.19. 3D Mesh: The total number of 150 000 FEs is used in cover plate of 1 600 kVA distribution transformer without SSI.

Table 5.7. The measured, analytical and numerical calculated stray losses in tank cover

I (A)	Measured Losses [10] (W)	Analytical Cal. Losses (W)	3D FEM Cal. Losses (W)	%
1 000	246	247	245.8	0.09
1 500	487	555	553	13.5
2 000	917	987	983	7.2
2 500	1 442	1 542	1 594	10.5

The investigations have been performed for four different currents of power transformer and the achieved results are shown in Table 5.7 and Figure 5.20 where the results of analytical and numerical calculations of eddy current losses have been compared with the experimental results [10].

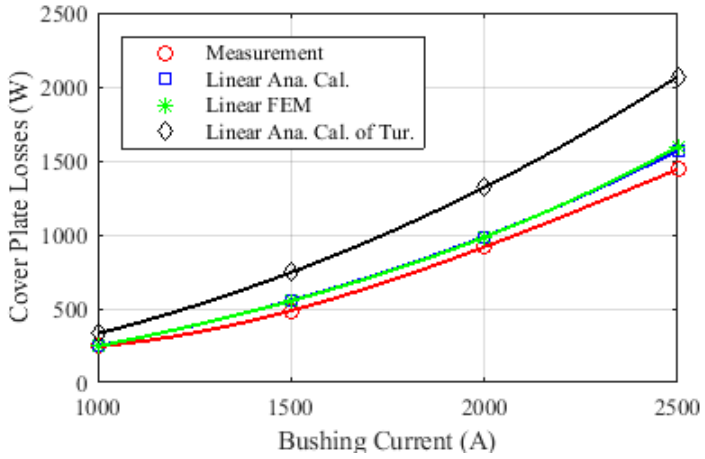

Figure 5.20. Comparison of eddy current losses obtained from different methods

Diamond and circle marker symbol in Figure 5.20 shows the linear model calculations and measurement of cover losses respectively by Turowski [10], but asterisk and square ones denote calculation results of stray losses by the 3D FEM and AM, respectively, in the case of linear material. Solid lines have been obtained based on a cubic spline interpolation using MATLAB library. The analytical calculations of losses have been done in Field Calculator Interface of Maxwell software by using equations (2.24) and (2.19).

It is evident that there is a good agreement between the results of the measured and the numerical methods (maximum error of estimate is %13.5) and it demonstrates the validity of the 3D FEM linear calculations for estimation of cover plate losses. There is also considerable agreement between the calculated losses in linear model of AM and 3D FEM. Therefore, the mesh number used in the 3D FEM simulation is acceptable to simulate the problem.

Equation (2.24) demonstrates that the leakage losses of transformer cover varies with the square of conductor current. But experimental results of losses in large power transformers as seen in Table 5.7 and in Figure 5.20 show that the induced tank losses vary less than the current squared as Deuring [50] has been demonstrated.

The stray losses of five 3-phase distribution transformers at different rates obtained by numerical and analytical computations have been shown in Table 5.8. The comparison of them shows a good agreement.

Table 5.8. Numerical and analytical calculated stray losses in tank cover of 3-phase distribution transformers without SSI

S (kVA)	*I* (A)	*A* (mm)	*D* (mm)	Stray Loss Cal. (W) Analytical	3D FEM	%
630	909	150	55	190	195	2.6
800	1 155	150	55	307	315	2.6
1 000	1 443	150	55	479	490	2.3
1 250	1 804	200	70	752	766	1.9
1 600	2 309	200	70	1 233	1 220	-1.1

The distance between the bushings, *A*, and the diameter of the bushing holes, *D*, have been determined according to the values of conductor current [51]. As we expected, there is a very good agreement between the 3D FEM and analytical method outcomes.

Table 5.9. 3D FEM calculated stray losses in tank cover of 3-phase distribution transformers with and without SSI

S (kVA)	*I* (A)	3D FEM Stray Loss Cal. (W) Without SSI	With SSI	%
1 000	1 443	490	354	-27.8
1 250	1 804	766	434.5	-43.3
1 600	2 309	1 220	454	-62.8

The comparison of 3D FEM calculated stray losses in tank cover of the 3-phase distribution transformers with and without SSI in Table 5.9. The results show a remarkable reduction in the losses because of small SSI.

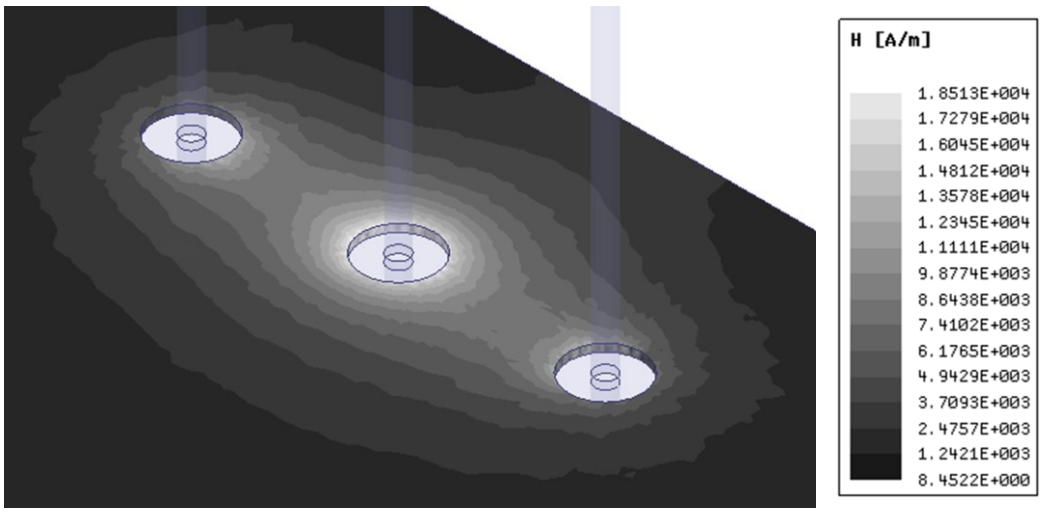

(a)

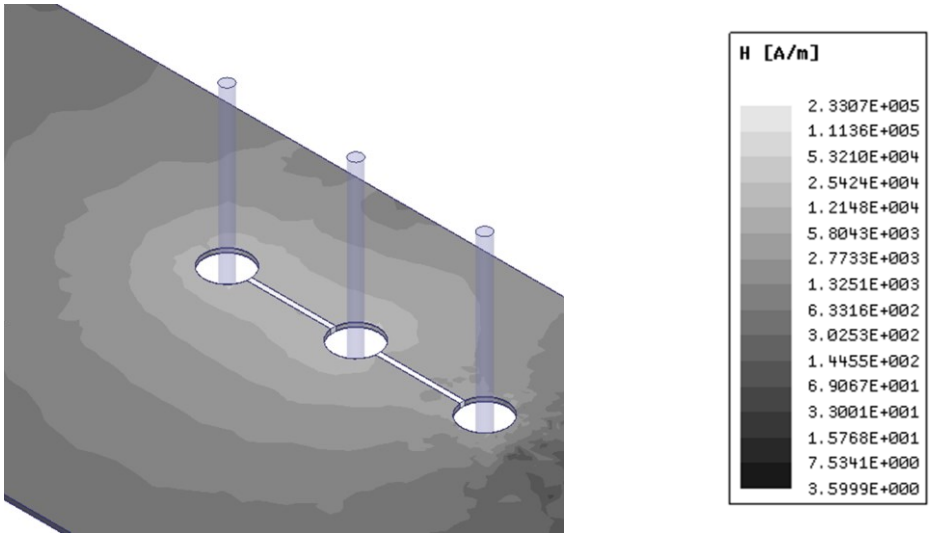

(b)

Figure 5.21. Magnetic field intensity in cover plate of 1 600 kVA 3-phase distribution transformer: a) without SSI b) with SSI

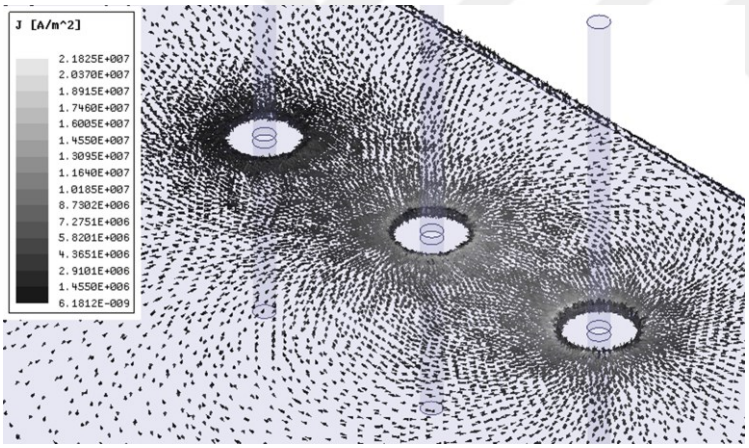

(a)

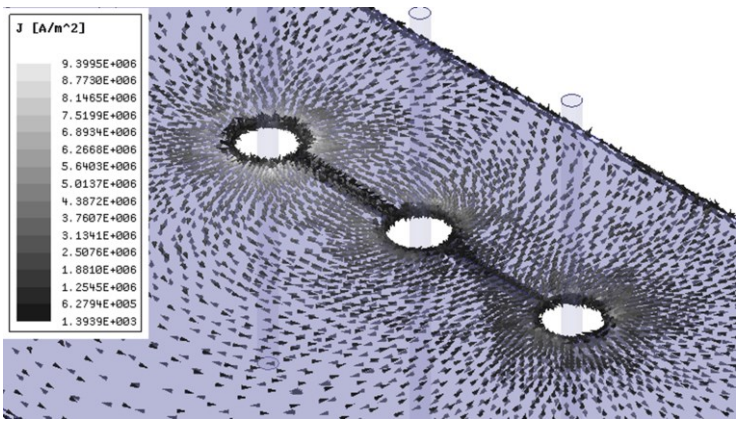

(b)

Figure 5.22. Eddy current density distribution in cover plate of 1600 kVA 3-phase distribution transformer: (a) without SSI (b) with SSI

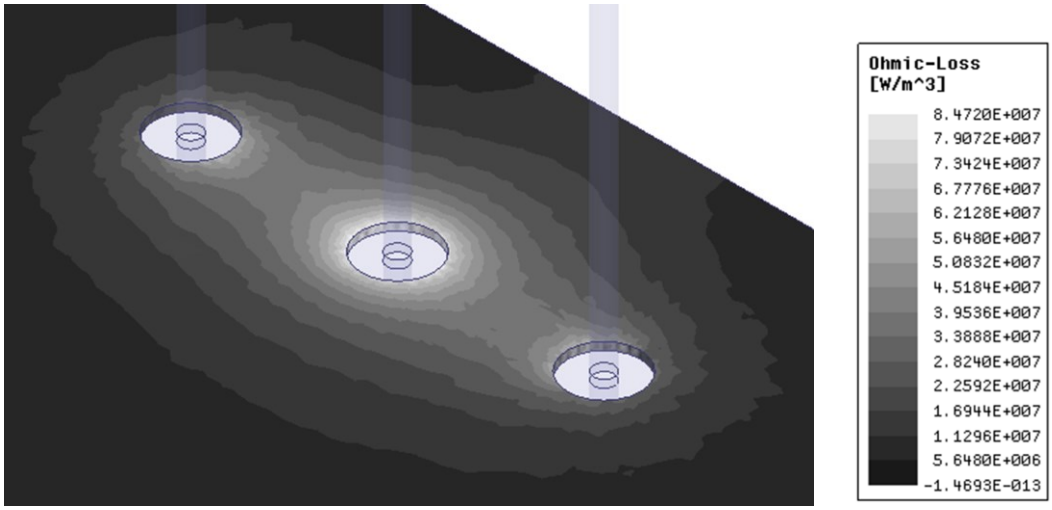

(a)

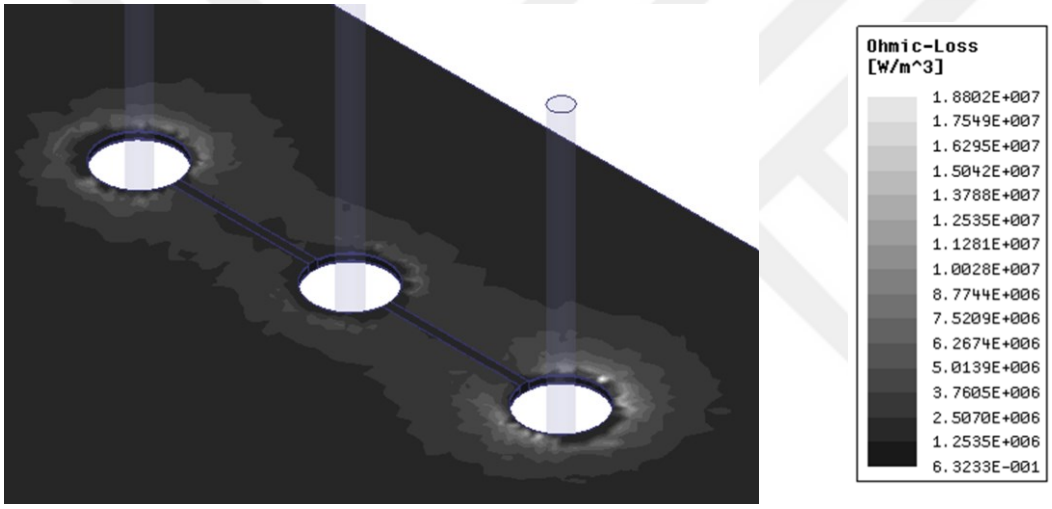

(b)

Figure 5.23. Stray losses in cover plate of 1600 kVA 3-phase distribution transformer: (a) without SSI (b) with SSI

There is a good agreement between the results of the magnetic field intensity and stray losses of the 3-phase transformer obtained from 3D FEM and analytical calculations as shown in Figure 5.21(a), Figure 5.5 and in Figure 5.23(a), Figure 5.6 respectively.

By using non-magnetic SSI between bushing holes the magnetic field intensity is considerably increased in this region in comparison to without SSI (depicted in Figure 5.21), but the stray losses is dramatically decreased (depicted in Figure 5.23) as well as eddy current distribution (depicted in Figure 5.22). In addition, the reduction of the losses can also be demonstrated by using Equation (2.19) whereas the magnitude of the losses are proportional to the root of permeability μ.

The temperature distribution of tank cover can be obtained by coupling the loss results obtained from Maxwell to ANSYS Steady-State Thermal [27]. The used thermal parameters has been given in Table 5.1. Since the cover plate is cooled by air as much as oil [25], therefore, we can assume that the plate is only cooled by air. Properties of the air film are dependent on its temperature (average temperature of the cover plate and air). So that, the convection heat transfer coefficient of cover plate according to Equation (2.39) can approximately be equal to 5[W/m^2.K].

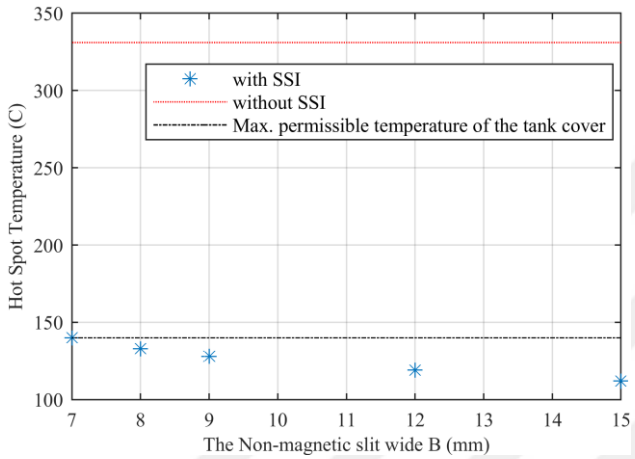

Figure 5.24. Numerical calculated hot spots in the tank cover of 1 600 kVA, 400 V three-phase distribution transformers with and without SSI

As it is clear from Table 5.10, the hot spot temperature of the cover plates for a 3-phase transformer with a power rating less than 1 000 kVA is not critical. The applied steps for the optimal design of tank cover for a 1 600 kVA, 400 V 3-phase distribution transformer is given in Table 5.10 and Figure 5.24. Obviously, after a few steps one can find the minimum SSI wide in the transformer cover plate at the design stage.

Table 5.10. Numerical calculated hot spots in tank cover of 400 V three-phase distribution transformers with and without SSI

S (kVA)	*I* (A)	Hot spot Temp. (˚C)	SSI wide *B* (mm)	Reduced Hot Spot Temp. (˚C)
1 000	1 443	174	1	118
1 250	1 804	231	2	134
1 600	2 309	331	15	112
1 600	2 309	331	12	119
1 600	2 309	331	9	128
1 600	2 309	331	8	133
1 600	2 309	331	7	140

As a result, temperature distribution over the cover plate surface of 1 600 kVA 3-phase distribution transformer is illustrated in Figure 5.25 in the case of (a) without SSI and (b) with SSI where the non-magnetic slit wide is 8 mm.

According to the simulation results given in Table 5.9, Table 5.10 there is significant reduction at the stray losses (from 1 220 to 454W) and therefore at the hot spot temperature (from 331 to 133˚C) in the cover plate while using small SSI.

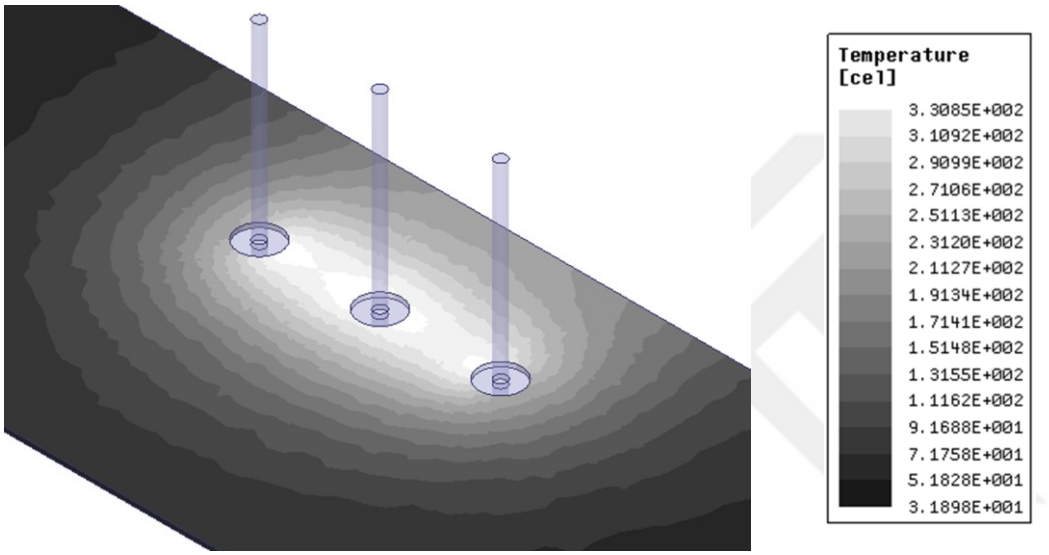

(a)

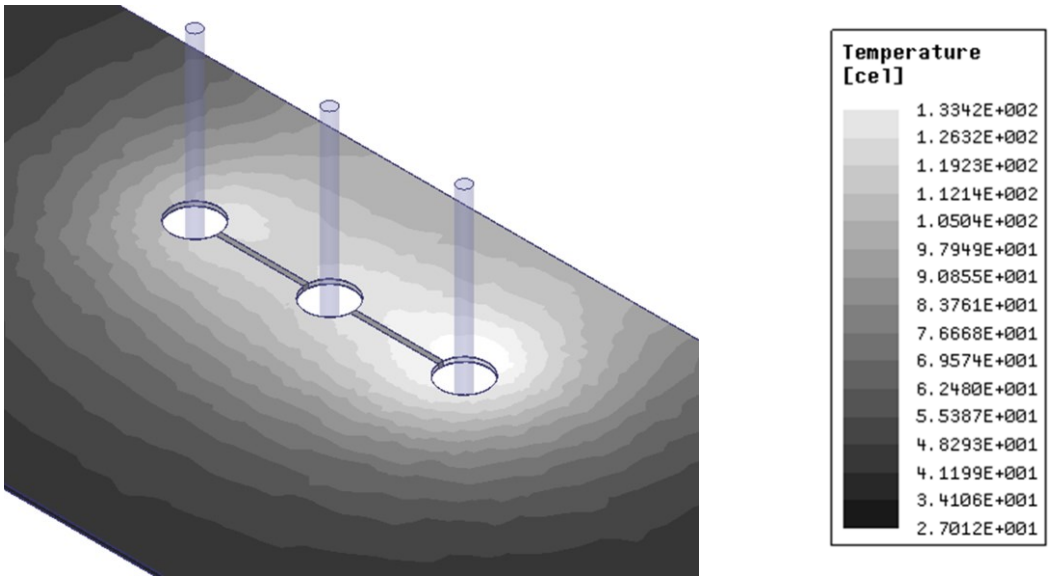

(b)

Figure 5.25. Temperature distribution in cover plate surface of 1 600 kVA 3-phase distribution transformer: (a) without SSI (b) with SSI (8 mm)

The used simulation time for each iteration to calculate the hot spot temperature is about 40min in a system with configuration of Intel Core i3 1st Gen. 370M (2.4 GHz) processor, and 8GB RAM Memory. Therefore, by the use of the considered system the optimal design after a few iterations has been done, to find the minimum wide of SSI.

Transient non-linear magneto-thermal FEM results

The total number of 240 000 FEs were used in the simulated model.

Table 5.11. The measured, analytical and numerical calculated stray losses in tank cover

Current, [A]	Measured Losses, [W] [1]	Linear FEM Cal. of losses, [W] $\mu_r = 500$	Non-linear FEM Cal.	
			Losses, [W]	Error, [%]
1 000	246	252	257	4.5
1 500	487	566	546	12
2 000	917	1 006	926	1
2 500	1 442	1 572	1 395	-3.3

The investigations were performed for four different currents of power transformer and the results achieved are shown in Table 5.11. The results of analytical and numerical calculations of eddy current losses have been compared with the experimental results in Table 5.11 and Figure 5.26.

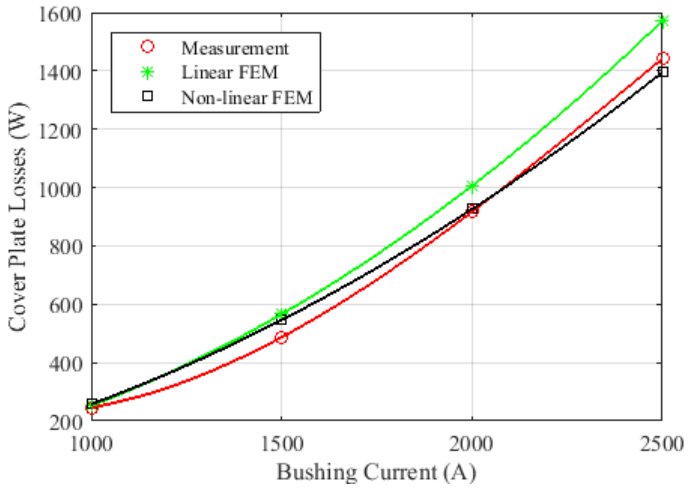

Figure 5.26. Comparison of eddy current losses obtained from different methods.

The average percent error between non-linear FEM and experiment results of the eddy losses is about 3.6.

losses with the non-linear analytic method and experimental results[10] given in Figure 5.33. The average error of the results is about 0.28%, as given in Table 5.16, while using only 1800 adaptive FEs mesh over the cover plate, which shows the accuracy and good speed of the FEM simulations.

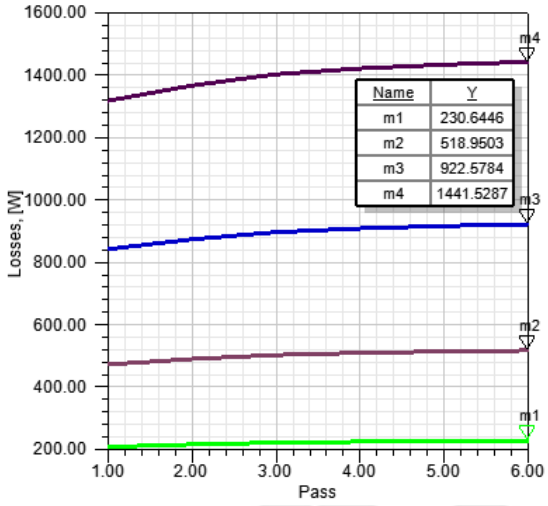

Figure 5.32. Adaptive FEM losses of the cover plate in six iterations for different currents.

Table 5.16. The measured, analytical and numerical calculated stray losses in tank cover

I (A)	Measured losses [10], (W)	Non-linear analytical cal. of losses [10], (W)	3D FEM cal. of losses (W)	%
1 000	246	247	231	-6.1
1 500	487	555	519	6.57
2 000	917	987	923	0.65
2 500	1 442	1 542	1 442	0

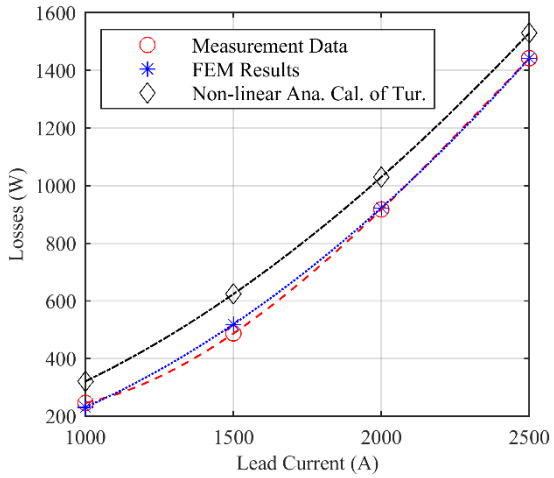

Figure 5.33. Comparison between cover losses obtained by the FEM, non-linear analytic method and measurement[10], for different currents.

Eddy losses of tank cover obtained from the FEM results show a non-linear behavior with respect to current in Figure 5.33.

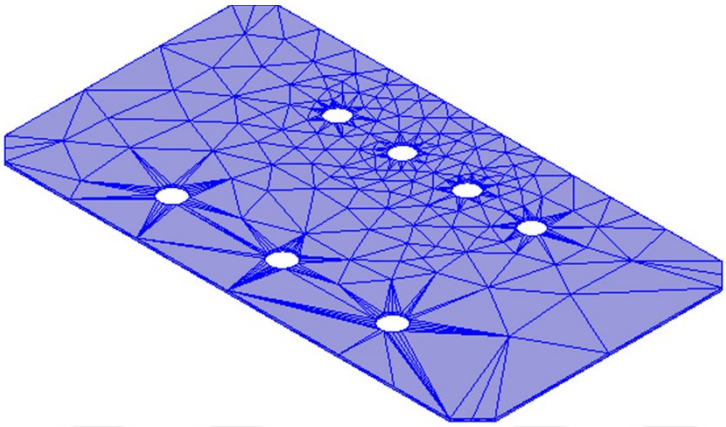

Figure 5.34. 1800 FEs adaptive mesh over the cover plate

Temperature curves for the cover plate without SSI are determined using parametric studies in this section. The current *I* was varied from 0.4kA to 3.7kA using intervals of 0.3kA for distribution transformers.

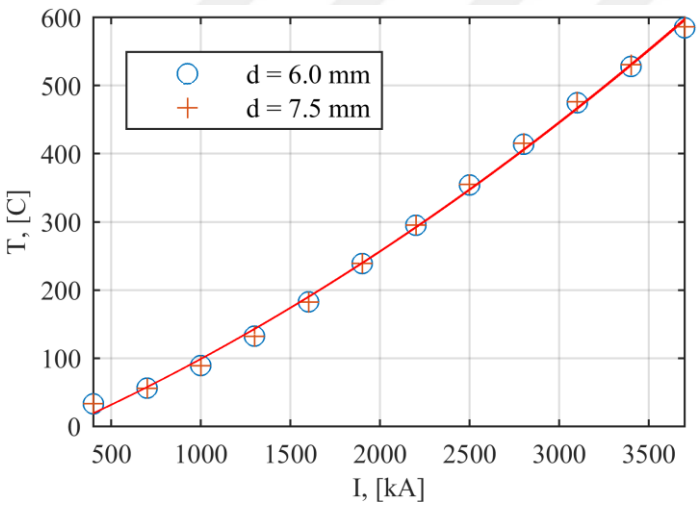

Figure 5.35. Temperature curves for cover plate without SSI

The hot spot temperature of the cover plate without SSI for different thickness (6mm and 7.5mm), obtained from FEM simulations, depicted in Figure 5.35. It reveals that the losses and hot spot temperature of the cover is independent of the thickness if the thickness is greater than 1.82mm, two times of the skin depth number (0.91mm). The eddy losses become smaller if the plate thickness is less than 1.82mm. The results are applicable only for a steel conductor with electrical conductivity of 6.8×10^{6}[S/m] and relative magnetic permeability

of 500 [24]. FEM temperature distribution of the cover for the case of I = 1.4434kA has been given in Figure 5.36(a), where the hot spot temperature is 153.9°C. The maximum temperature value in the tank cover T=600°C is calculated, i.e. dangerous temperature values or hot spots are developed in the cover plate which could lead to further failures on the transformer.

Temperature curves with SSI

The temperature of the cover plate with SSI, B=1mm, for the case of I = 1.443 4 kA has shown in Figure 5.36(b). The hot spot temperature, which is 106°C, has been reduced under the permissible temperature.

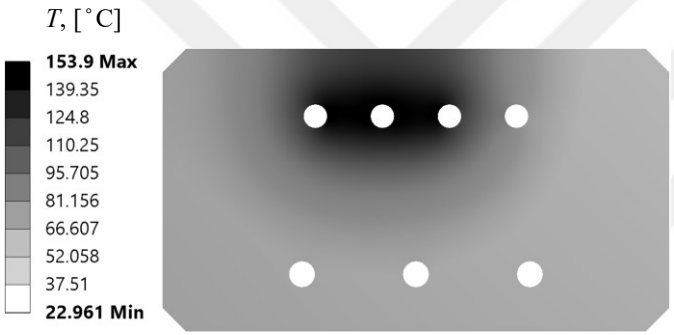

(a)

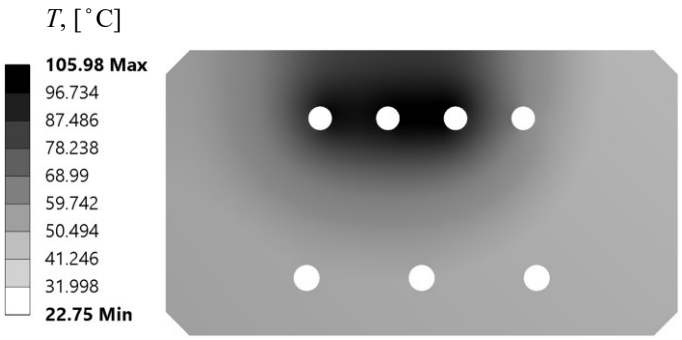

(b)

Figure 5.36. Temperature distribution in cover plate for I = 1.443kA : a) without SSI; b) with SSI (B = 1 mm).

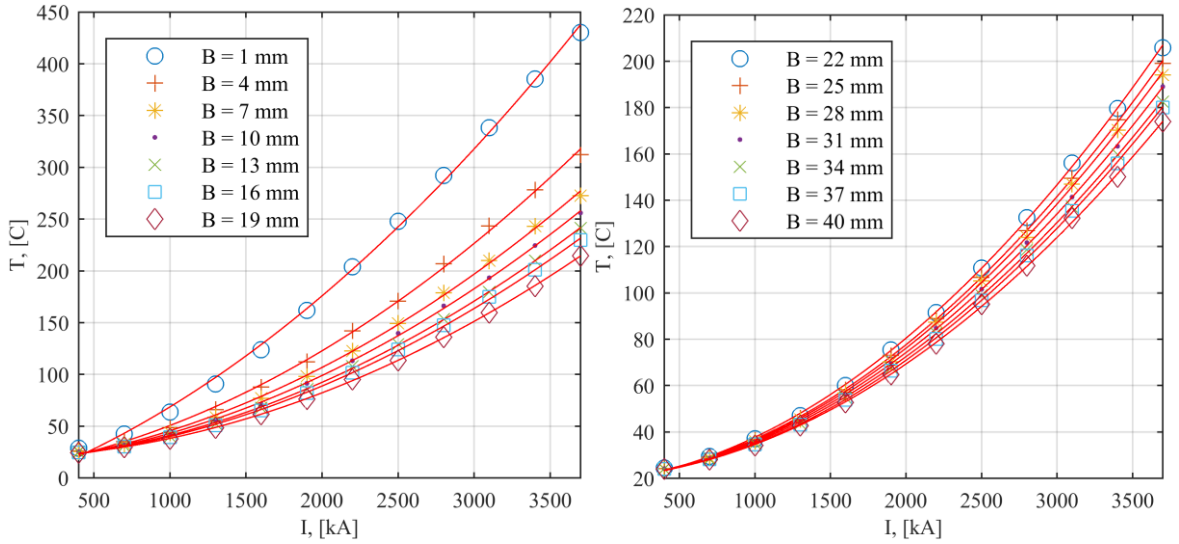

(a) (b)

Figure 5.37. Hot spot temperature curves for cover plate with (a) thin (b) thick SSI slit

Analytic formulas of the hot spot temperature

Taking into consideration equations (2.19) and (2.24), it can be concluded that the losses and then the temperature of the cover plate are directly proportional to the square of the source current. Therefore, it may be to extend the FEM simulations results to a general form of a quadratic analytic formula as (5.1).

$$T = aI^2 + bI + c \tag{5.1}$$

where T is the hot spot temperature of the cover (°C), I is the lead current of the bushing conductors, a, b and c are coefficients obtained by fitting equation (5.1) to the temperature data showed in Figure 5.35 and Figure 5.37 in the previous sections. According to previous section, there is no change in the temperature of the tank cover if the cover thickness is greater than 1.82mm. So that, equation (5.1) is independent of the tank cover thickness. Coefficients of the analytic formula have been given in Table 5.17 and Table 5.18 for the tank cover plate without and with SSI respectively.

This analytic formula can be used to obtain the hot spot temperature in tank covers of different distribution transformers.

Table 5.17. Coefficients of the temperature curve for the tank cover plate without SSI (Curve of Figure 5.35)

B, [mm]	$a \times 10^{-4}$	*b*	*c*
0	0.2180	0.082 0	0.528 2

Table 5.18. Coefficients of the temperature curve for the tank cover plate with SSI (Curves of Figure 5.37)

B, [mm]	$a \times 10^{-4}$	*b*	*c*
1	0.206 1	0.0401	10.806 8
4	0.172 8	0.017 9	16.852 3
7	0.155 8	0.012 7	18.303 8
10	0.148 4	0.009 9	19.110 1
13	0.142 1	0.007 6	19.905 0
16	0.136 4	0.006 9	20.004 8
19	0.128 6	0.004 8	20.834 7
22	0.121 9	0.005 5	20.458 9
25	0.119 4	0.004 4	20.856 2
28	0.116 2	0.004 3	20.775 0
31	0.111 5	0.004 3	20.862 6
34	0.107 8	0.004 1	20.847 3
37	0.107 7	0.003 3	21.146 1
40	0.102 3	0.003 6	21.066 7

Table 5.19. Temperatures in the tank cover plate without SSI.

Rating(kVA)	*I*, [kA]	*T*, [˚C] FEM	*T*, [˚C] Formula	%Error
1 000	1.443	153.9	164.8	7.1
1 250	1.804	218.2	223.1	2.2
1 600	2.309	308.9	311.6	0.87

Table 5.20. Temperatures in the tank cover plate with SSI.

Rating(kVA)	*I*, [kA]	*B*, [mm]	*T*, [˚C] FEM	*T*, [˚C] Formula	%Error
1 000	1.443	1	106	111.9	5.5
1 250	1.804	4	105.41	106.2	0.74
1 600	2.309	16	107.94	109.2	1.2

The proposed analytical equation (5.1) has been applied for six 3-phase distribution transformers in Table 5.19 and Table 5.20. in the case of without and with SSI respectively. The maximum percent error between the both methods is about 7.1 which it is possible to reduce the error by increasing the mesh.

5.4. FD Analysis of the Bushing Region

A magneto-thermal FD analysis in the bushing regions of the tank cover has been proposed in this section. The magnetic 2D FD analysis is based on the solution of Maxwell's equations at the cross section area in axial symmetry page of a steel disk considering linear/non-linear magnetic permeability, which is the novelty introduced in this work. To validate the results, the authors have been investigated the leakage flux in the tank cover not only in terms of a FD analysis of the losses but also in terms of a FD/FE analysis of the temperature.

In the first section, transient magnetic FD and thermal FE analysis of the disk plate have been studied. In the next section, an adaptive magnetic FD steady state analysis and then a new thermal ADI-FD analysis of the disk have been proposed.

Finally, the results are compared with those of FEM and experimental results.

5.4.1. The magneto-thermal FD-FE analysis

The FDM magnetic analysis has been done at $N_z = 60$, $N_r = 300$ finite differences mesh in *z* and *r*-direction, respectively.

The transient linear magnetic FDM solution

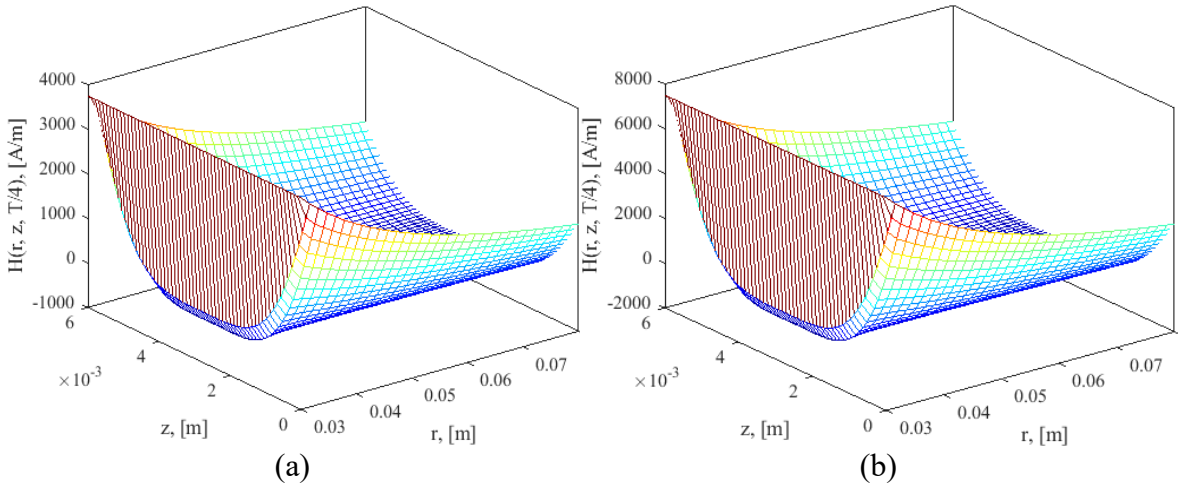

Figure 5.38. 2D FDM steady state waveforms of magnetic field intensity in the solution area for (a) 500, (b) 1 000A.

We can check the proposed method by calculating the magnetic field intensity and eddy current losses at the constant magnetic permeability in Figure 5.38 and Figure 5.40.

A comparison between FDM, FEM and AM results of magnetic field intensity in the center of steel disk for 500 and 1 000 A currents has been depicted in Figure 5.39. AM based solution of the magnetic field intensity in the center of steel disk has been obtained using (2.12).

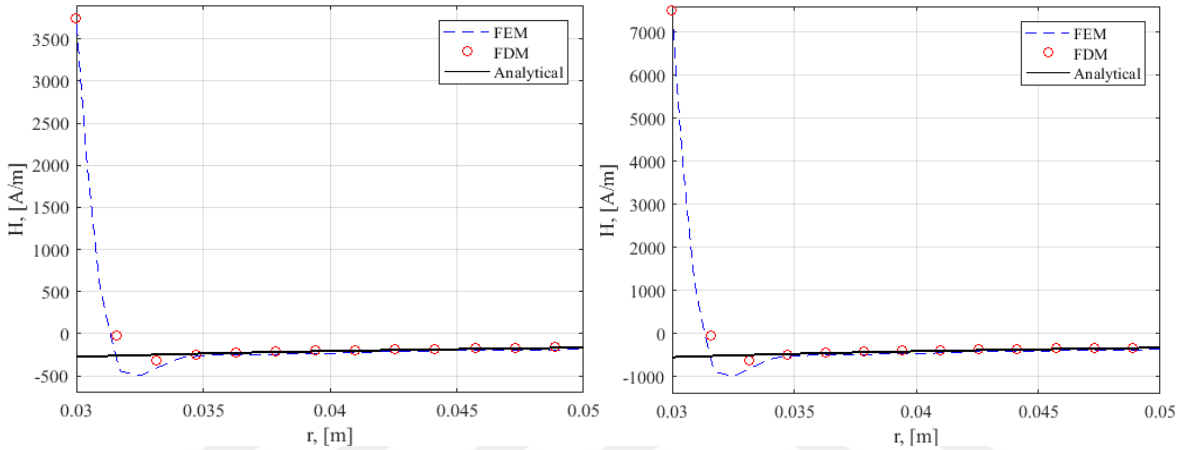

Figure 5.39. Comparison between the magnetic field intensities in the center of steel disk obtained at steady state condition by FDM, FEM and AM in the case of (a) 500 and (b) 1000 A.

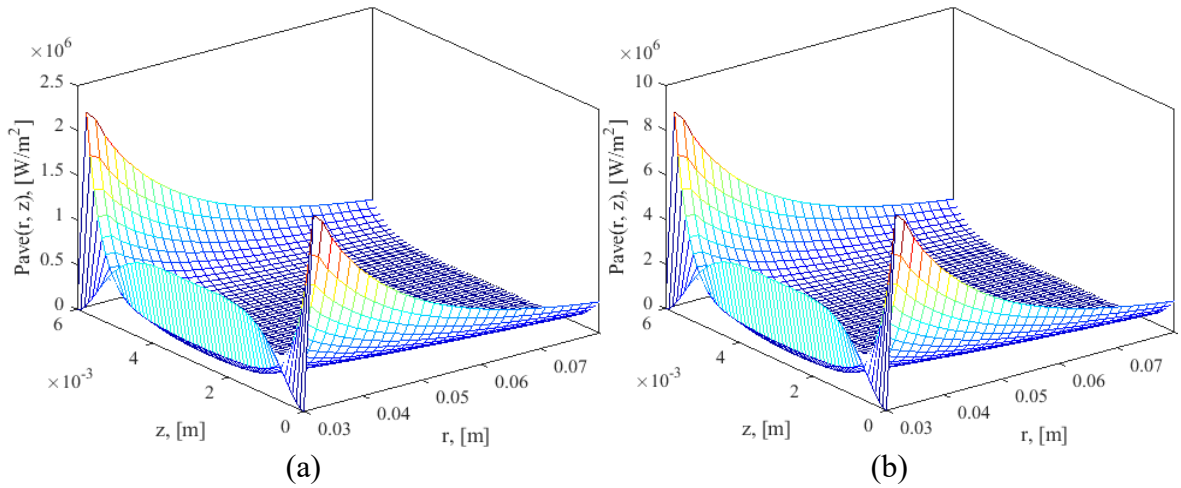

Figure 5.40. 2D FDM steady state waveforms of eddy losses in the solution area for (a) 500, (b) 1 000 A.

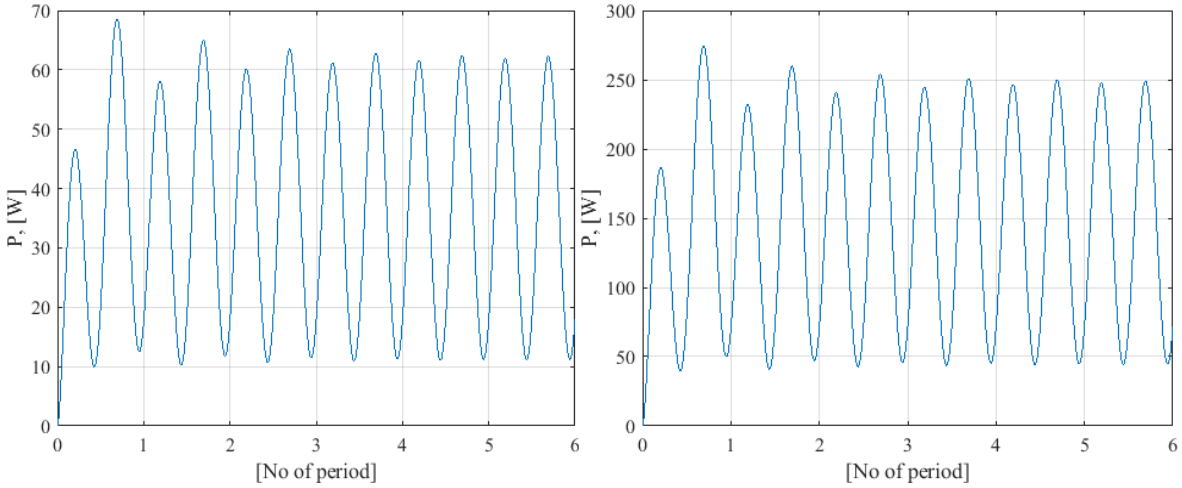

Figure 5.41. 2D FDM transient solution of the eddy losses of the disk for (a) 500, (b) 1000 A.

Table 5.21. Linear eddy current losses, [W] of the steel disk

	Mesh	Linear, P_{total}		
Current, [A]	$N_r \times N_z$	FDM	FEM	Analytic
500	100×30	36	36.8	36.06
500	300×60	35.8	36.8	36.06
1 000	100×30	143.9	147.25	144.3
1 000	300×60	146.44	147.25	144.3

The FD losses results are compared with those obtained from AM using (2.16) in Table 5.21. There is about 1.4% error due to the applied mesh numbers (18 000 FDs), which shows the efficiency of the method.

The transient non-linear magnetic FDM solution

FD solution of magnetic field intensity and magnetic field density given in Figure 5.42 and Figure 5.43 respectively taking into account non-linear magnetic permeability of the steel.

Table 5.22. Eddy current losses, [W] of the steel disk

	Linear, P_{total}			Non-linear, P_{total}	
Current, [A]	FDM	FEM	Analytic	FDM	FEM
500	36.6	36.8	36.06	34.1	31.5
1 000	146.4	147.25	144.3	131.1	124.87

The thermal FEM solution

Transient hot spot temperature on the hole surface at z = 3mm is presented in Figure 5.46 , which shows within 3 hours the disk temperature reaches to the steady state conditions.

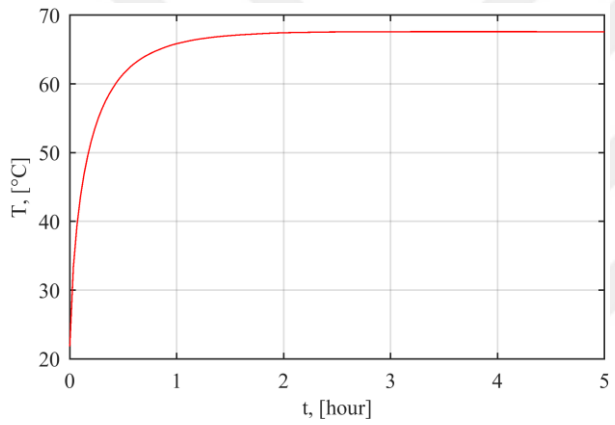

Figure 5.46. 2D FDM transient hot spot temperature on the hole surface at z = 3mm for 1000A.

The results obtained from non-linear FD analysis are then compared with those of FE software like ANSYS possessing axisymmetric.

Table 5.23. Hot spot temperature, [°C] on the hole surface, $r = a$.

	z = 3mm			z = 6mm		
Current, [A]	FDM	FEM	Abs. error	FDM	FEM	Abs. error
500	35.106	34.118	1	35.1	34.115	1
1 000	67.59	67.678	-0.09	67.57	67.661	-0.09

The numerical method based estimated temperature values are given in Table 5.23, for two different cases of 500 and 1 000 A current at two solution points of ($r = a$, z = 3mm) and ($r = a$, z = 6mm). According to the results, the small absolute error between both methods

verifies the FDM based solution. In addition, almost the same temperature along the thickness of the disk plate reveals that at the thermal analysis the cover thickness can be ignored.

The FD transient and steady state temperature distribution on the cross section surface of the disk given in Figure 5.46 and Figure 5.47 have been calculated by the heat conduction equation. It can be observed in Figure 5.47 and Figure 5.18 that the FD temperature distribution of the disk is as well as FF based calculation.

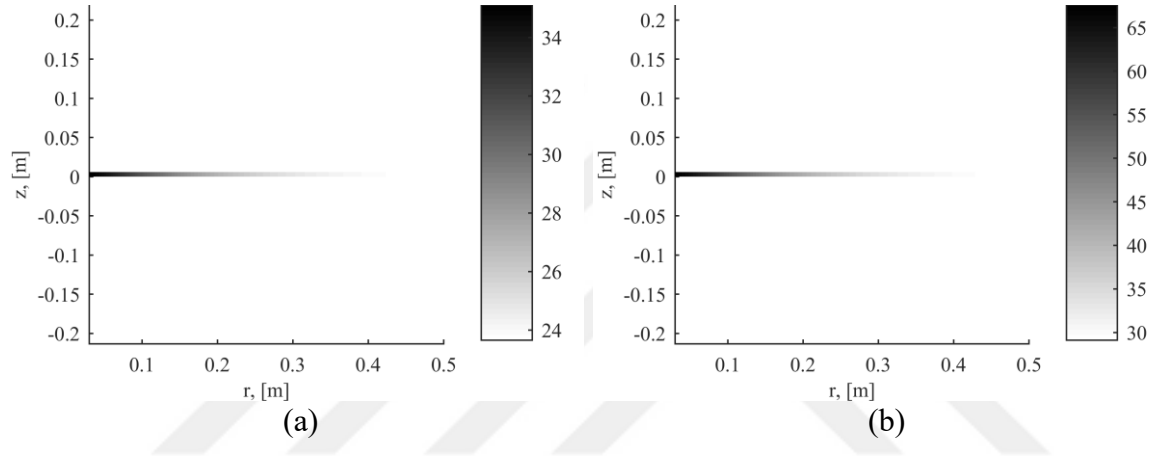

Figure 5.47. 2D FDM steady state temperature distribution on the cross section surface of the disk for (a) 500, (b) 1 000A.

The comparison between FDM, FEM and experimental results

Linear/non-linear FDM temperature distributions in the center of the disk thickness, z = 3mm, for bushing currents of 500 and 1 000 A are presented in Figure 5.48 and Figure 5.49. The results are verified by the experimental results[19, 22]. The FDM results has a better approximation in comparison with those of FEM, which verifies the non-linear FDM losses results in Table 5.22. According to Figure 5.48(a), the error of non-linear FDM and those of experiment is about -1.5°C for the case of 500A operation. The error between results of the non-linear FDM and those of experiments is about -0.03%, for the case of 1 000A operation as shown in Figure 5.48(b). It is also observed in Figure 5.49 the difference between the temperature obtained by linear FDM and FEM is very small for the case of 1 000A operation, as may be predicted from Table 5.22.

The another importance of comparing of linear and nonlinear cases for 1000A operation is that the error between nonlinear FDM and FEM with those of linear FDM and FEM is decreasing with increasing of magnetic fields. This is due to the fact that the *B-H* curves of both linear and nonlinear operations for lower values of magnetic fields (far from the bushings) is very near to each other. For the higher values of magnetic field, the error between linear and nonlinear cases of operation is getting high and this is due to increasing of error of *B-H* curves for higher values of the magnetic field. Though the error between linear and nonlinear cases is low for regions far from the bushings but the losses of these region are not considerable high and consequently is not important [10, 20].

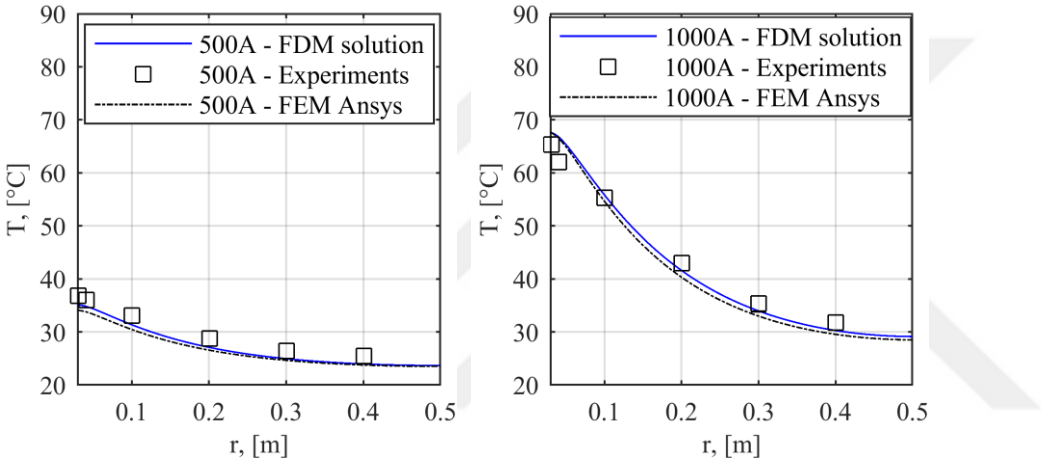

Figure 5.48. The temperature distribution of the disk plate obtained by the non-linear FDM, FEM and experiment for (a) 500, (b) 1 000 A.

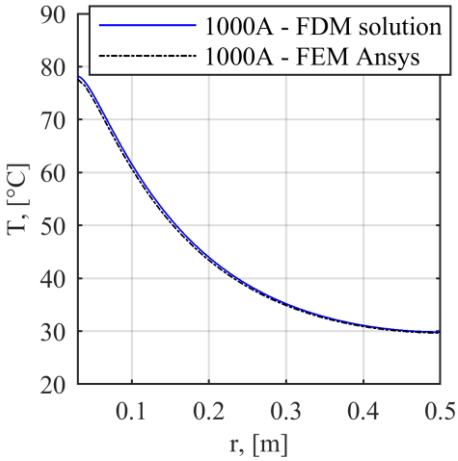

Figure 5.49. The temperature distribution of the disk plate obtained by the linear FDM and FEM for 1 000 A.

5.4.2. The adaptive magneto-thermal ADI-FD analysis

The adaptive FD solution of the magnetic field quantity $H_\varphi(r,z)$ in the transformer cover plate under the linear and non-linear magnetic permeability condition starts with an initial grid of 900 points ($N_z = 15$, $N_r = 60$ points in z and r-axes, respectively) in the first level mesh and continuous by increasing mesh grid 7.36 times in the skin depth region.

The linear adaptive magnetic FD steady-state analysis

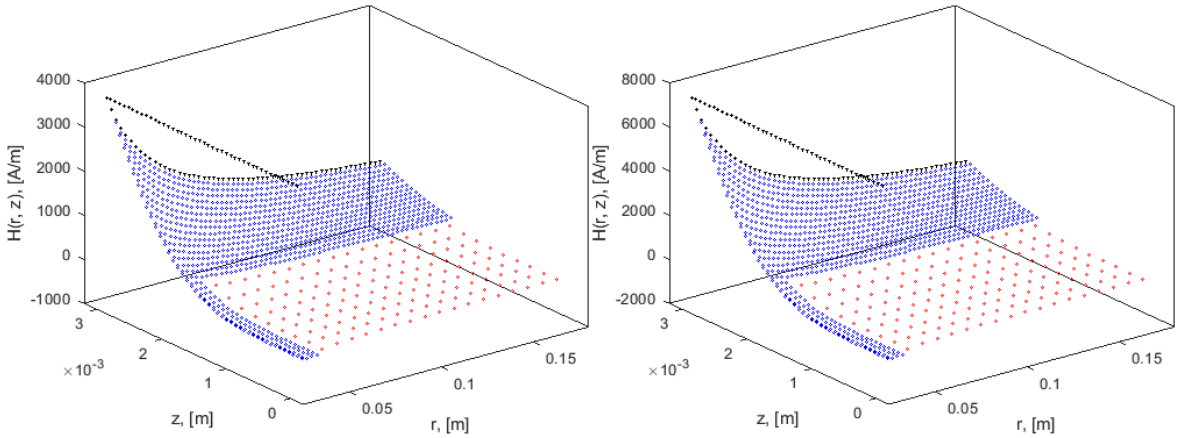

(a) (b)

Figure 5.50. Waveforms of magnetic field intensity at steady state conditions. 2D FDM: (a) 500A, (b) 1 000 A.

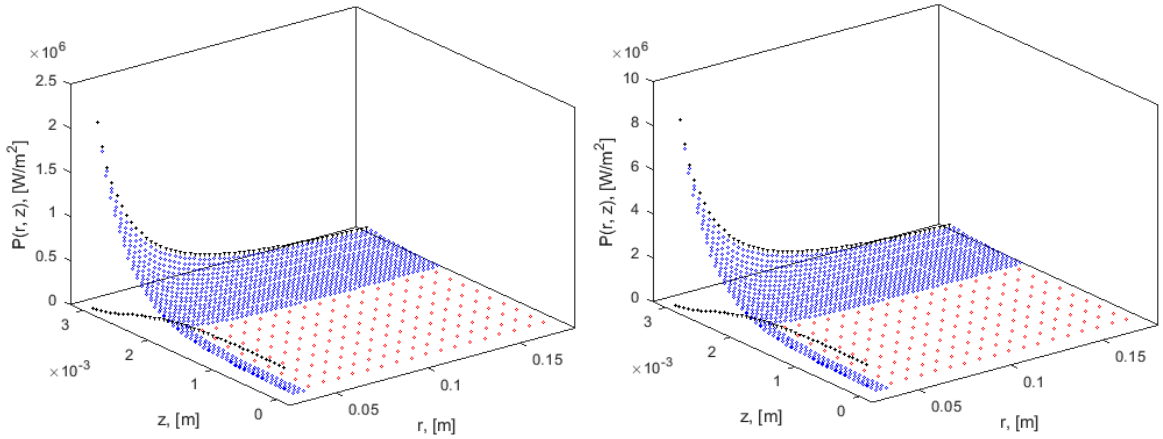

(a) (b)

Figure 5.51. Waveforms of eddy losses distribution at steady state conditions. 2D FDM: (a) 500A (b) 1 000 A.

The linear steady state solution of 3D waveforms of the magnetic field quantity $H_\varphi(r,z)$ and its corresponding magnetic flux intensity $B_\varphi(r,z)$ of the cover plate at the two currents of 500 and 1 000A have been shown in Figure 5.50 and Figure 5.51, respectively.

The FD numbers used in the case of initial, 2-level-adaptive and fine mesh are 900, 3 683 and 7 832 respectively. At linear solution, the magnetic permeability is 900. The results of the linear calculations of losses in Table 5.24 reveal that the percent error between 2-level adaptive FDM and analytic method[16] is about 0.8%, which it verify the used mesh.

Table 5.24. Linear eddy current losses, [W] of the cover plate

Current, [A]	FDM losses			FEM Losses	Analytic losses	Error, [%]
	Initial mesh	Adaptive mesh	Fine mesh			
500	34.86	35.78	36	36.8	36.1	0.8
1 000	139.4	143.14	143.95	147.25	144.3	0.8

Table 5.25. Computational time, [s] of the linear analysis

Current, [A]	Adaptive mesh	Fine mesh	Ratio
500	122	887	7.3
1 000	136	1149	8.45

The non-linear adaptive magnetic FD steady-state analysis

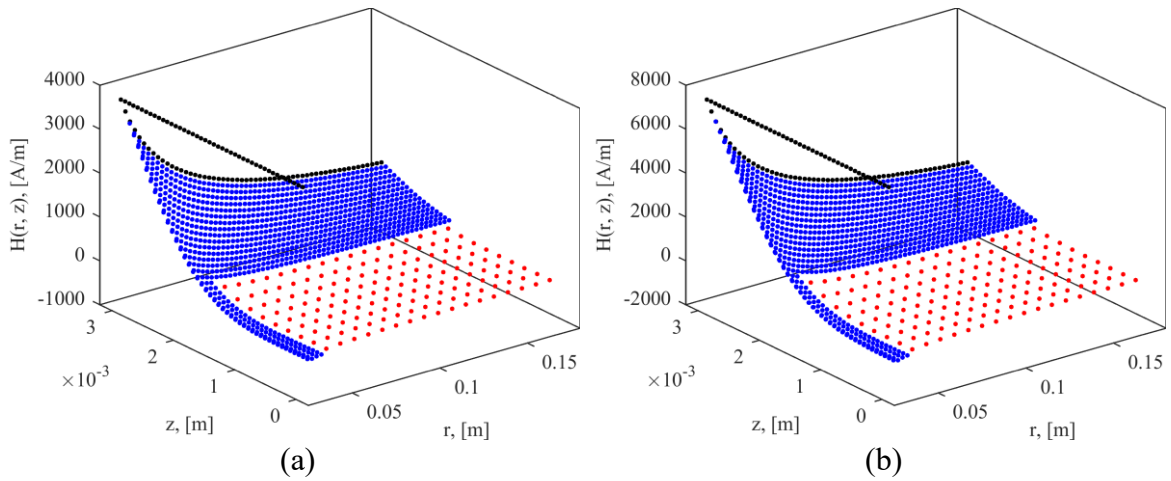

Figure 5.52. Waveforms of magnetic field intensity of the cover plate at steady state conditions. Adaptive 2D FDM: (a) 500A, (b) 1 000 A.

The non-linear steady state solutions of 3D waveforms of the magnetic field intensity $H_{\varphi}(r,z)$ and magnetic flux density $B_{\varphi}(r,z)$ of the cover plate at the two currents of 500 and 1 000 A have been shown in Figure 5.52 and Figure 5.53, respectively.

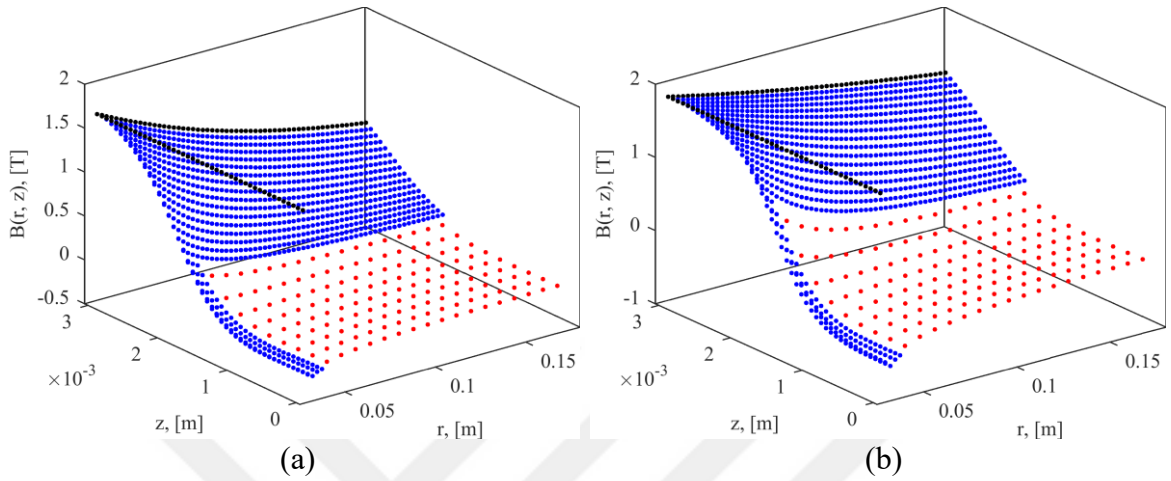

Figure 5.53. Waveforms of magnetic flux density of the cover plate at steady state conditions. Adaptive 2D FDM: (a) 500A, (b) 1 000 A.

The steady state solutions of the density of cover losses at the both currents have been showed in Figure 5.54. These reveal that, losses density is high at the penetration depth near the bushing region and significantly low in the other regions. In the case of 1 000 A, stray losses percent in the skin depth region is about 92% and in other regions is 8%. In addition, the magnetic field and cover losses rapidly vanished in the middle region of the plate, where used coarse mesh. The fine mesh is used for domains with large gradient of magnetic field intensity or wherein there are significant losses.

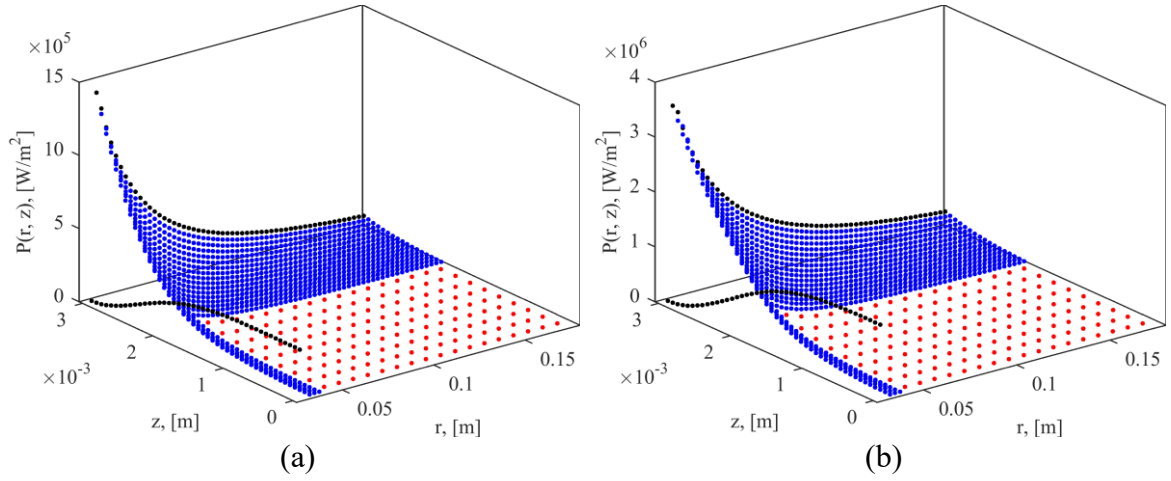

Figure 5.54. Waveforms of eddy losses distribution at steady state conditions. 2D adaptive FDM: (a) 500A, (b) 1 000 A.

The non-linear adaptive FDM results are then compared with those of non-linear FEM results which obtained from a FE software like ANSYS [27] possessing axisymmetric.

A general comparison between the applied numerical methods has been given in Table 5.26, where runtime, memory and mesh size of the models have been compared. It reveals that for simple model calculation FDM in comparison with FEM decreases the computational cost, significantly.

Table 5.26. Non-linear magnetic adaptive FDM vs FEM performance for 1 000A current

Method	Runtime, [s]	Memory	Mesh No.
FDM	490	886KB	3 683
FEM	5 130	561.8MB	36 700

A comparison between losses obtained from non-linear FDM and FE analysis have been given in Table 5.27. It is not clear which values are more accurate. However, a comparison between thermal results with experimental data may be determined the precision of the FDM results. In addition, according to losses results in Table 5.24 and Table 5.27, though the used FDs number and the computational time of fine mesh analysis are bigger than those for adaptive mesh approach are, there is no significant difference between the accuracy of the losses.

Table 5.27. The non-liner calculated eddy current losses, [W], of cover plate

Current, [A]	FDM losses			FEM losses
	Initial mesh	Adaptive mesh	Fine mesh	
500	34.39	35.21	35.41	31.5
1 000	132	134.86	135.63	124.87

Table 5.28. The computation time, [s], of the analysis

Current, [A]	Linear			Non-linear		
	Adaptive mesh	Fine mesh	Ratio	Adaptive mesh	Fine mesh	Ratio
500	122	887	7.3	279	2 628	9.4
1 000	136	1 149	8.45	490	4 804	9.8

The thermal ADI-FDM solution

According to the results of the transient ADI-FDM solution, the hot spot temperature of the cover plate for the both current values of 500 and 1 000 A (Figure 5.5), the cover plate temperature reaches to the steady state condition after about 3 hours.

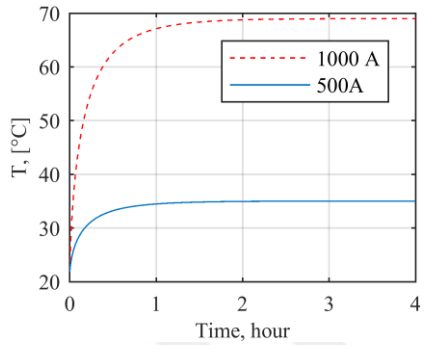

Figure 5.55. ADI Transient solution of hot spot temperature of the cover plate at z =6mm.

The steady state temperature distributions of the disk based on the numerical computations have been presented in Figure 5.56 and Figure 5.57. One can find FDM temperature distribution of disk is as well as FE based.

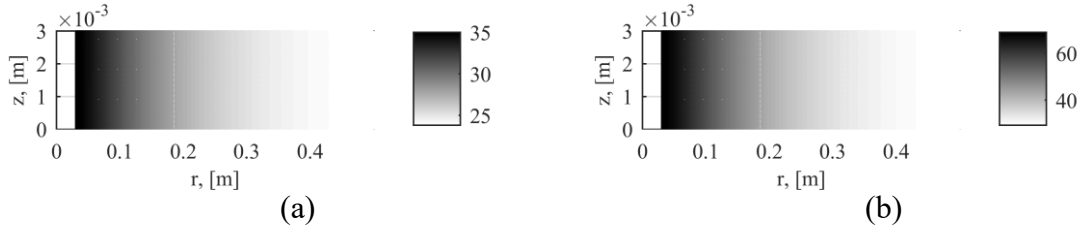

Figure 5.56. Steady state temperature distribution on the cover plate cross section area. 2D ADI-FDM: (a) 500A and (b) 1 000A.

The comparison between FDM, FEM and experimental results

The ADI-FDM temperature distribution of losses at the top surface of the plate (z = 6mm) for two different currents are presented in Figure 5.57. It is shown that for 1 000 A the FDM results are in a very good agreement with those of FEM. The results are also verified by the experimental results[19, 22]. The average error is about 1 percent. There is about 1°C error between the FDM and experimental results, for the case of 500 A.

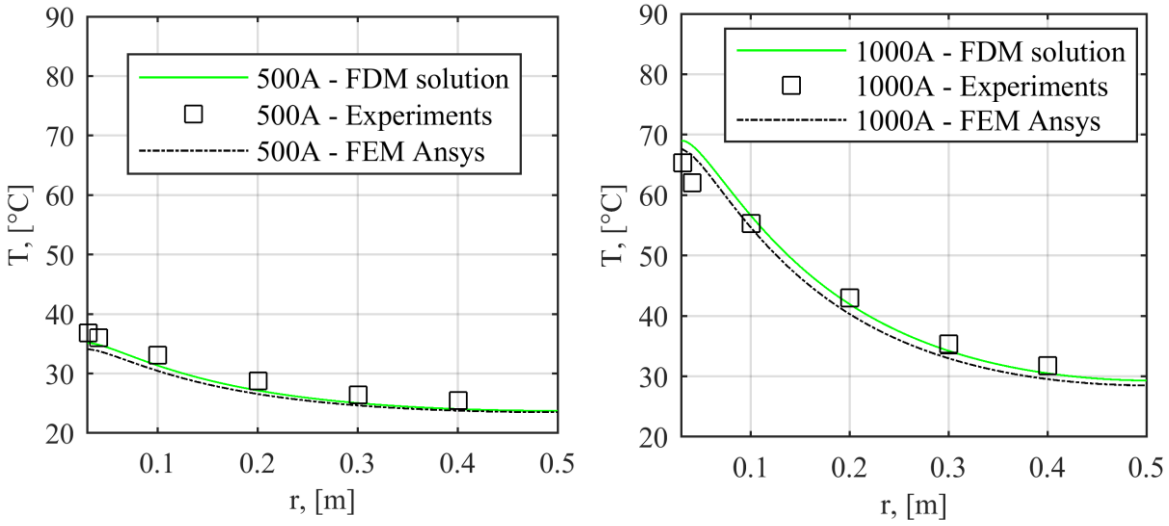

(a) (b)

Figure 5.57. The ADI-FDM, FEM and experimental results of temperature distribution on the top surface of the disk, z = 6 mm, for 500 and 1 000 A.

Therefore, according to Table 5.26 and Figure 5.57, FDM results in comparison with FEM gives better estimates in spite of the fact that FD analysis has been done with less mesh, memory and lower computational time.

6. CONCLUSIONS

Hot spot temperature of the transformer cover plate because of high current bushings has been studied in this research.

Linear and nonlinear behavior of the magnetic permeability of the cover steel considered to find out the accurate estimation of its losses and temperature.

3D Linear analytical magnetic analysis of the problem, at first as a good approximation of the cover plate, in the bushing regions and then in the tank cover has been presented with MATLAB code.

Transient non-linear magnetic FD analysis at the bushing region of the transformers cover has been developed in MATLAB programming language. The magnetic field and power losses analysis of the transformer cover have been studied using 2D FDM in different currents of 500 and 1000 A, with the considering nonlinear behavior of the cover steel.

On initial step of investigation, comparison of the magnetic field and eddy losses outcomes from linear FEM and FDM calculations with those obtained from linear AM shows a good adaptation.

The power losses obtained from these analyses have been used into heat conduction equation in the thermal analysis in the PDE Tools of MATLAB, which solves PDEs using FEM. The thermal results got from the proposed method are compared with those obtained from ANSYS/Maxwell program. Comparing the results of 2D FDM with those obtained from FEM and experiments confirms the efficiency and capability of the FDM approach in solving and analyzing non-linear problems and FDM is more flexible than FEM to deal with the nonlinear constitutive law.

In addition, a new adaptive magneto-thermal FD analysis near the bushing region of transformers cover has been proposed in this research to develop a model of the magnetic field, the eddy losses and the temperature distribution, accurately, taking into account the nonlinear/linear magnetic permeability of the cover steel. The assumptions, the magnetic and thermal boundary conditions have been presented, clearly. The formulas of the non-

linear/linear adaptive magnetic FDM and the thermal ADI-FDM in the bushing regions of the transformer cover has been explained in details. The FDM algorithm has also been developed by MATLAB code.

Furthermore, using the FD local adaptive mesh technology instead of fine mesh method gives fast solution with better adaptation to the experiment results without losing the resolution. Thermal analysis of the model has been done by applying ADI-FDM due to the fact that ADI is a fast algorithm compared to the other schemes (Explicit, Implicit and Crank-Nicolson schemes). Combination of adaptive-mesh technology and ADI-FDM not only could improve the computational accuracy but also decrease the computational cost and has a stable solution.

Comparing the adaptive FDM results with those of FEM simulation and experimental results reveals the superior efficiency and capability of the applied numerical method. Apart from that, it shows that the FDM has the following advantages; i- FDM is more flexible to deal with the nonlinear constitutive law than FEM, ii- it is the most popular method for simple geometric regions, iii- FDM is easy to implement and iv- it has low-cost computational design procedure.

The proposed formula can also be applied for estimating magnetic distribution, losses and temperature distribution in the wall of transformer tank. The proposed 2D FDM, developed in this study has easy usage feature and lower computational process. With the considering the economical point there is no need for using powerful programs or costly licenses of specialized software. The results of the proposed method can be used to improve the cover plate design and the efficiency of transformers.

A linear/non-linear 3D FEM optimization design of cover plates for a 1600 kVA, 400 V 3-phase distribution transformer has also proposed in this study. In order to overcome to the local overheating and keeping the maximum temperature below 140 °C, a suitable geometry of SSI slit has been applied between the bushing regions. Eddy losses and hot spot temperature of the cover plate have been estimated in the case of with and without SSI. According to the results there is a considerable agreement between the losses in 3D FEM, AMs and experimental results. Considerable reduction in the cover plate losses and hot spot

temperature has been seen when using a very thin SSI slit. The applied linear approximation is sufficiently fast to do the computations in a moderate computer resource.

Counter-posing non-linear results to the linear case, reveals the non-linear FEM solution has more accurate results than the linear FEM solution, but the run times of calculations is vice versa.

As a result, we can use safely a linear design of tank cover, since the outcome of the linear stray losses and maximum temperature are higher than non-linear and experiment results. Especially, for fast electromagnetic analyses, a linear surface impedance boundary condition can be used to model the carbon steel tank cover.

This study also has proposed a fast estimation for the calculation of hot spot temperatures reached in distribution transformers cover, using surface impedance boundary condition at linear losses computations. 3D FEM simulations are applied to calculate the maximum temperature attained in the carbon steel of transformer cover with and without SSI.

According to the FEM hot spot temperature curves, the maximum bushing current to keep the hot spot temperature below 140℃ can be easily determined. Therefore, it can help distribution transformer manufacturers to specify the optimum design of transformers cover. The agreement between the losses obtained from 3D FEM and experimental results verify the applied estimation method. Thus, the proposed analytical results are accurate, and can improve the design time of distribution transformers cover.

REFERENCES

1. Olivares-Galván, Juan C, Georgilakis, Pavlos S, and Ocon-Valdez, Rodrigo. (2009). A review of transformer losses. *Electric Power Components and Systems*, 37 (9), 1046-1062.

2. Olivares-Galván, JC, Magdaleno-Adame, S, Escarela-Perez, R, Ocon-Valdéz, R, Georgilakis, PS, and Loizos, G. 2012. *Experimental validation of a new methodology to reduce hot spots on the screws of power transformer tanks*. Electrical Machines (ICEM), 2012 XXth International Conference on.

3. Olivares-Galvan, Juan Carlos, Magdaleno-Adame, Salvador, Escarela-Perez, Rafael, Ocon-Valdez, Rodrigo, Georgilakis, Pavlos S, and Loizos, George. (2014). Reduction of stray losses in flange–bolt regions of large power transformer tanks. *IEEE Trans. on Industrial Electronics*, 61 (8), 4455-4463.

4. Magdaleno-Adame, S, Olivares-Galvan, JC, Escarela, R, Raichenko, O, and Kladas, AG. 2014. *Hot spots mitigation on tank wall of a power transformer using electromagnetic shields*. Electrical Machines (ICEM), 2014 International Conference on.

5. Zahedi, M. Zia, and Iskender, I. (2016). 3D FEM Optimal Design of Transformer Cover Plates to Decrease Stray Losses and Hot Spot Temperature. *International Journal on Technical and Physical Problems of Engineering (IJTPE)*, 8 (3), 56-60.

6. Fani, Bahador, Golshan, MEH, Abyaneh, HA, and Saghaian-nejad, M. (2011). A runs test-based method for discrimination between internal faults and inrush currents in power transformers. *International Trans. on Electrical Energy Systems*, 21 (3), 1392-1408.

7. Bigdeli, Mehdi, Vakilian, Mehdi, and Rahimpour, Ebrahim. (2013). A probabilistic neural network classifier-based method for transformer winding fault identification through its transfer function measurement. *International Trans. on Electrical Energy Systems*, 23 (3), 392-404.

8. Board, I. (1995). *IEEE Guide for Loading Mineral-Oil-Immersed Transformers*. IEEE Standard C, 57, 1-112.

9. McShane, C Patrick. (2001). Relative properties of the new combustion-resist vegetable-oil-based dielectric coolants for distribution and power transformers. *IEEE Trans. on Industry Applications*, 37 (4), 1132-1139.

10. Turowski, J., and Pelikant, A. (1997). Eddy Currents Losses and Hot-Spot Evaluation in Cover Plates of Power Transformers. *Proc. Inst. Elect. Eng. Elect. Power Appl.*, 144 (6), 435-440.

11. Magdaleno-Adame, S., Escarela-Perez, R., Olivares-Galvan, J. C., Campero-Littlewood, Eduardo, and Ocon-Valdez, and Rodrigo. (2014). Temperature Reduction in the Clamping Bolt Zone of Shunt Reactors: Design Enhancements. *IEEE Trans. on Power Delivery*, 29, 2648-2655.

12. Olivares, J.C., Perez, R. Escarela, Kulkarni, S.V., Leon, F. de, Vasquez, E. Melgoza, and Anaya, O. Hernandez. (2004). Improved Insert Geometry for Reducing Tank-Wall Losses in Pad-Mounted Transformers. *IEEE Trans. on Power Delivery*, 19 (3), 1120-1126.

13. Olivares, J.C., Perez, R. Escarela, Kulkarni, S.V., Leon, F. de, and Vega, M.A. Venegas. (2004). 2D Finite-Element Determination of Tank Wall Losses in Pad-Mounted Transformers. *Electric Power Systems Research*, 71, 179-185.

14. Galvan, J.C. Olivares, Adame, S. Magdaleno, Littlewood, E. Campero, Perez, R. Escarela, and Georgilakis, P.S. (2011). Techno-Economic Evaluation of Reduction of Low Voltage Bushings Diameter in Single-Phase Distribution Transformers. *Electric Power Components and Systems*, 39, 1388-1402.

15. Maximov, Serguei, Escarela-Perez, Rafael, Olivares-Galvan, Juan Carlos, Guzman, Salvador Juan, and Campero-Littlewood, Eduardo. (2016). New Analytical Formula for Temperature Assessment on Transformer Tanks. *IEEE Trans. on Power Delivery*, 31 (3), 1122-1131.

16. Vecchio, R. M. Del, Poulin, B., Feghali, P. T., Shah, D. M., and Ahuja, R. (2010). *Transformer Design Principles: With Applications to Core-Form Power Transformers*. Boca Raton, FL: USA: CRC Press, 500-506.

17. Maximov, Serguei, Olivares-Galvan, Juan Carlos, Magdaleno-Adame, Salvador, Escarela-Perez, Rafael, and Campero-Littlewood, Eduardo. (2015). New Analytical Formulas for Electromagnetic Field and Eddy Current Losses in Bushing Regions of Transformers. *IEEE Trans. on Magnetics*, 51, 6300710.

18. Magdaleno-Adame, Salvador, Olivares-Galvan, Juan Carlos, Penabad-Duran, Patricia, Escarela-Perez, Rafael, and Lopez-García, Irvin. (2015). Fast computation of hot spots temperature due to high current cable leads in power transformers tank walls. *International Trans. on Electrical Energy Systems*, 25 (12), 3374-3383.

19. Lopez-Fernandez, X. M., Penabad-Duran, P., Turowski, J., and Ribeiro, P. M. (2012). Non-linear heating hazard assessment on transformer covers and tank walls. *Przeglad Elektrotech*. (Elect. Rev.), 88 (7b), 28–31.

20. Vecchio, R. M. Del, and Ahuja, R. (2013). Analytic Nonlinear Correction to the Impedance Boundary Condition. *IEEE Trans. on Magnetics*, 49 (12), 5687–5691.

21. S. Maximov, R. Escarela Perez, Adame, S. Magdaleno, Galvan, J.C. Olivares, and Littlewood, E. Campero. (2015). Calculation of Nonlinear Electromagnetic Fields in the Steel Wall Vicinity of Transformer Bushings. *IEEE Trans. on Magnetics*, 51 (6), 6300811.

22. Fernandez, X.M. Lopez, Duran, P. Penabad, and Turowski, J. (2012). Three Dimensional Methodology for the Overheating Hazard Assessment on Transformer Covers. *IEEE Trans. Industry Applications*, 48, 1549-1555.

23. Durana, P. Penabad, Fernandez, X.M. Lopez, and Turowski, J. (2015). 3D Non-Linear Magneto-Thermal Behavior on Transformer Covers. *Electric Power Systems Research*, 121, 333-340.

24. Kulkarni, Shrikrishna V, and Khaparde, SA. (2004). *Transformer Engineering: Design and Practice*. Vol. 25: CRC Press, 134-178.

25. Turowski, Janusz. (2014). *Engineering Electodynamics: Electric Machine*. CRC Press, 417-433.

26. Sadiku, Matthew N.O. (2011). *Elements of electromagnetics*. New York: Oxford University Press, 369-440.

27. Inc., ANSYS. 2012. *User's Guide - Maxwell 3D/ANSYS Maxwell*. Canonsburg, PA, USA, 1-1006.

28. Internet: Börlin, Niclas. Nonlinear Optimization Trust-region methods. URL: http://www.webcitation.org/query?url=https%3A%2F%2Fwww8.cs.umu.se%2Fkurser%2F5DA001%2FHT07%2Flectures%2Ftrust-handouts.pdf&date=2019-01-22, Accessed : 22.01.2019.

29. Buljak, Vladimir. (2011). *Inverse analyses with model reduction: proper orthogonal decomposition in structural mechanics*. Springer Science & Business Media, 19-84.

30. Turowski, J. (1993). *Technical Electrodynamics*. Warsaw, Poland: WNT.

31. Filippopoulos, G., and Tsanakas, D. (2005). Analytical Calculation of the Magnetic Field Produced by Electric Power Lines. *IEEE Trans. on Power Delivery*, 20,1474-1482.

32. Holman, J.P. (2010). *Heat transfer*. New York: McGraw-Hill, 327-344.

33. Internet: MathWorks. Heat Distribution in a Circular Cylindrical Rod. URL: http://www.webcitation.org/query?url=https%3A%2F%2Fwww.mathworks.com%2Fhelp%2Fpde%2Fexamples%2Fheat-distribution-in-a-circular-cylindrical-rod.html%3Fs_tid%3Dsrchtitle&date=2019-01-22, Accessed : 22.01.2019.

34. Weigen, Chen, Chong, Pan, and Yuxin, Yun. (2009). Power transformer top-oil temperature model based on thermal–electric analogy theory. *International Trans. on Electrical Energy Systems*, 19 (3), 341-354.

35. Georgilakis, Pavlos Stylianos. (2009). *Spotlight on modern transformer design*. Springer Science & Business Media.

36. Biro, Oszkar, and Preis, Kurt. (1989). On the use of the magnetic vector potential in the finite-element analysis of three-dimensional eddy currents. *IEEE Trans. on Magnetics*, 25 (4), 3145-3159.

37. Preis, K, Bardi, I, Biro, O, Magele, C, Vrisk, G, and Richter, KR. (1992). Different finite element formulations of 3D magnetostatic fields. *IEEE Trans. on Magnetics*, 28 (2), 1056-1059.

38. Elmoudi, Asaad A. (2006). *Evaluation of power system harmonic effects on transformers: Hot spot calculation and loss of life estimation.* Doctoral Dissertation, Helsinki University of Technology, Helsinki, 8-28.

39. Internet: MathWorks. Partial Differential Equation Toolbox. URL: http://www.webcitation.org/query?url=https%3A%2F%2Fwww.mathworks.com%2Fhelp%2Fpde%2Findex.html&date=2019-01-22, Accessed : 22.01.2019.

40. Sadiku, Matthew N. O. (2001). *Numerical techniques in electromagnetics*. New York: CRC Press, 121-235.

41. Gillott, D. H., and Calvert, J. F. (1965). Eddy current loss in saturated solid magnetic plates, rods, and conductors. *IEEE Trans. on Magnetics*, 1 (2),126–137.

42. Internet: MathWorks. Nonlinear Heat Transfer in a Thin Plate. URL: http://www.webcitation.org/query?url=https%3A%2F%2Fwww.mathworks.com%2Fhelp%2Fpde%2Fexamples%2Fnonlinear-heat-transfer-in-a-thin-plate.html&date=2019-01-22, Accessed : 22.01.2019.

43. He, Zhi Zhu, Xue, Xu, and Liu, Jing. (2013). An effective finite difference method for simulation of bioheat transfer in irregular tissues. *Journal of heat transfer*, 135 (7), 071003.

44. Srinivasa, Nandagopalan Auviur. (2006). *Adaptive mesh refinement for a finite difference scheme using a quadtree decomposition approach*. Master's Thesis, Texas A&M University, Texas, 1-22.

45. Chen, Han, Min, Chohong, and Gibou, Frédéric. (2007). A supra-convergent finite difference scheme for the Poisson and heat equations on irregular domains and non-graded adaptive Cartesian grids. *Journal of Scientific Computing*, 31 (1), 19-60.

46. Internet: MathWorks. Unconstrained Nonlinear Optimization Algorithms. URL: http://www.webcitation.org/query?url=https%3A%2F%2Fwww.mathworks.com%2Fhelp%2Foptim%2Fug%2Funconstrained-nonlinear-optimization-algorithms.html%23f3137&date=2019-01-22, Accessed : 22.01.2019.

47. Internet: Wikipedia. Alternating direction implicit method. URL: http://www.webcitation.org/query?url=https%3A%2F%2Fen.wikipedia.org%2Fwiki%2FAlternating_direction_implicit_method&date=2019-01-22, Accessed : 22.01.2019.

48. Patankar, Suhas. (1980). *Numerical heat transfer and fluid flow*. CRC press, 47-49.

49. Internet: MathWorks. Math. Graphics. Programming. URL: http://www.webcitation.org/query?url=https%3A%2F%2Fwww.mathworks.com%2Fproducts%2Fmatlab.html%3Fs_tid%3Dhp_products_matlab&date=2019-01-22, Accessed : 22.01.2019.

50. Deuring, W.G. (1957). Induced Losses in Steel Plates in the Presence of an Alternating Current. *AIEE Trans.*, 75,166-173.

51. Internet: ŞTİ., EREN ELEKTRİK SAN. VE TİC. LTD. EREN Trafo.URL: http://www.webcitation.org/query?url=http%3A%2F%2Fwww.erentrafo.com.tr%2F&date=2019-01-22, Accessed : 22.01.2019.

52. Holland, S, O'connell, GP, and Haydock, L. (1992). Calculating stray losses in power transformers using surface impedance with finite elements. *IEEE Trans. on Magnetics*, 28 (2), 1355-1358.

CURRICULUM VITAE

Personal Information

Surname, name	: ZAHEDI, Mohammad Zia
Nationality	: Afghanistan
Date and Place of Birth	: 04.04.1974, Wardak
Marital status	: Married
Tel	: 0 553 283 66 81
E-mail	: mzzahedi@gmail.com

Education

Degree	School/ Program	Graduated date
PhD	Gazi University/Electrical Electronics Eng.	Ongoing
Master	Shiraz University/Physics	2001
Undergraduate	Amirkabir University of technology/Physics	1997

Professional Experience

Year	Place of Work	Position
2002-2011	Kabul Polytechnic University	Assistant Prof.

Foreign Languages

English, Turkish

Publications

1. Zahedi, M. Z., Iskender, I. (2016). 3D FEM Optimal Design of Transformer Cover Plates to Decrease Stray Losses and Hot Spot Temperature. *International Journal on Technical and Physical Problems of Engineering, 8*(3), 56-60.

2. Zahedi, M. Z., Iskender, I. (2018). FDM Electromagnetic Analysis ın Bushing Regions of Transformer. *International Journal on Technical and Physical Problems of Engineering, 10*(1), 27-33.

3. Zahedi, M. Z., and Iskender, I. Non-Linear Eddy Current Loss and Thermal Analysis on Transformer Cover. *Gazı Unıversıty Journal of Scıence*, (Accepted 2018)

4. Zahedi, M. Z., and Iskender, I. (2018) The Non-Linear Adaptive FDM Magnetic and ADI-FDM Thermal Analysis on Covers Plate. *Journal of Thermal Science and Engineering Applications*, 11(1), 011010-1 - 011010-8, DOI: 10.1115/1.4041345.

5. Iskender, I, and Zahedi, M. Z. Fast calculation of hot spot temperature in transformer cover plate. *Electrical Engineering*, under review.

6. Zahedi, M. Z., and Iskender, I. Adaptive computation of eddy losses in transformer windings. *Electrical Engineering*, under review.

Hobbies

Swimming, Mountaineering, Playing Football and Table Tennis, Calligraphy, Programming, Reading, and Watching TV.

GAZİ GELECEKTİR...